Coupling Dynamics in Aircraft: A Historical Perspective

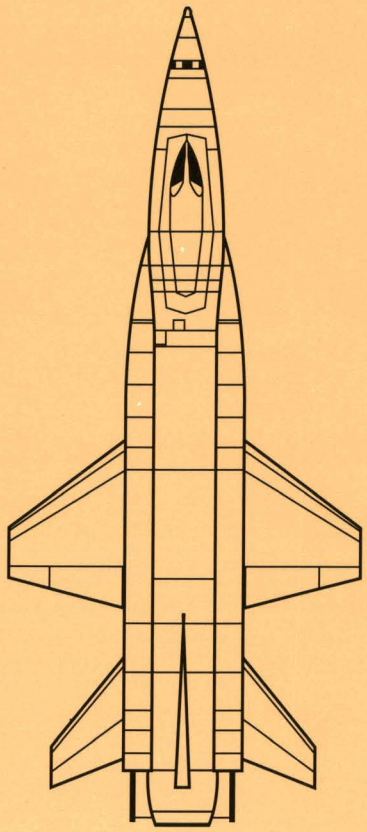

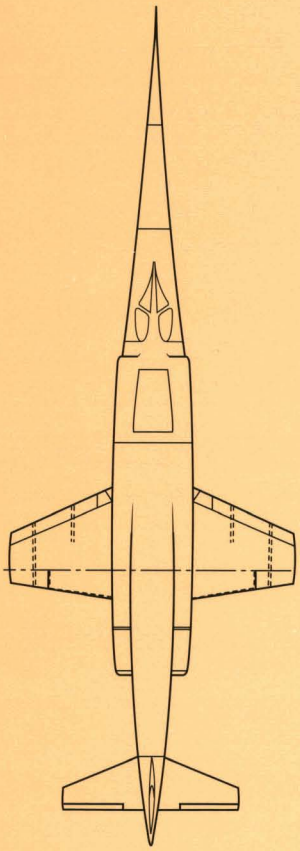

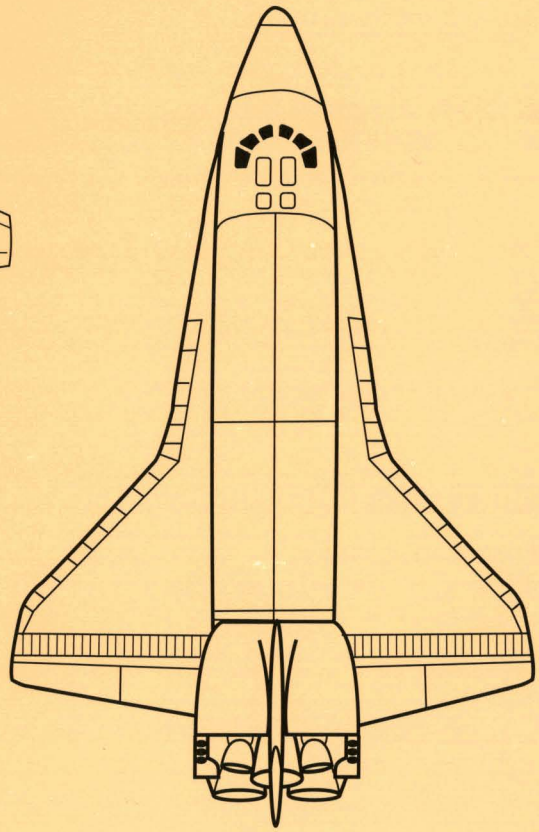

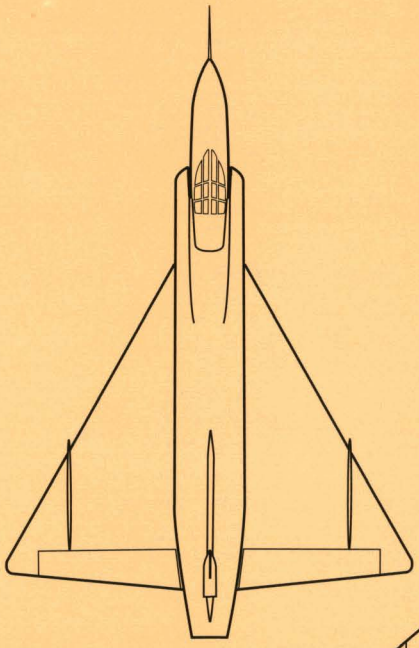

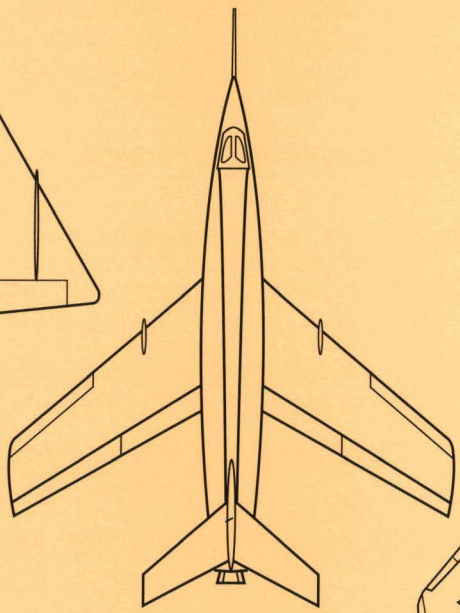

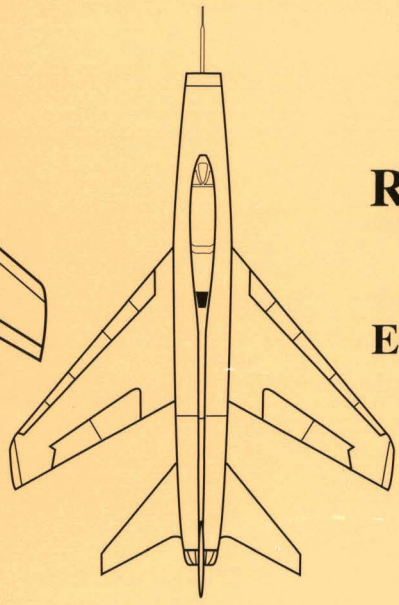

Richard E. Day
Dryden Flight Research Center
Edwards, California

NASA Special Publication 532

1997

Coupling Dynamics in Aircraft: A Historical Perspective

Richard E. Day
Dryden Flight Research Center
Edwards, California

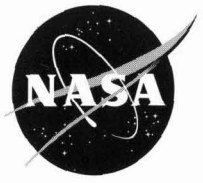

National Aeronautics and Space Administration

Office of Management

Scientific and Technical Information Program

CONTENTS

TABLES

FIGURES

FOREWORD

Richard E. (Dick) Day grew up in pre-World War II Indiana. As a young man, he participated in the pre-war Civilian Pilot Training program, receiving his pilot's license in 1938. Two years later, he joined the Royal Canadian Air Force and enrolled in the aviation cadet program there. After graduation, he served as a flight instructor in the RCAF.

After Pearl Harbor, he was allowed to transfer to the U.S. Army Air Corps. He flew 24 missions as a B-17 pilot in Europe and later served as a flight instructor back in the United States. In 1946, he returned to civilian life. He received his bachelor's degree in Physics and Mathematics from Indiana University in 1951.

After graduation from college, Dick joined the NACA High Speed Flight Station at Edwards, California, as an aeronautical research engineer. Among his early assignments were the X-1 rocket research aircraft and the XF-92 delta-wing research airplane.

In 1953, Day acquired access to the analog computer owned by the U.S. Air Force at Edwards Air Force Base. He programmed the computer with the characteristics of an airplane (as recorded by that airplane in flight), then added a control stick and a cathode ray tube which served as a pilot's display. Thus, he had constructed a rudimentary flight simulator.

Dick soon had his simulator programmed with the characteristics of the Bell X-2. Data from the most recent flight would be programmed into the simulator. Then, the estimated degradation in stability due to the proposed next increase in Mach number or angle of attack would be added to the program, and the pilot could estimate the controllability that the airplane would exhibit at the proposed flight condition. This was the first time that a test pilot was given a method to assess controllability of his airplane at some flight condition to be flown in the future.

Predictions were made for flight 13 of the X-2 which indicated that the airplane would experience control reversal if flown to high angle of attack at a speed in excess of Mach 2.4. On flight 13, the X-2 reached Mach 3.2, a speed much higher than predicted, and the pilot found himself flying past his landing site at a high rate of speed. A turn was initiated above Mach 2.4, and the limit angle of attack was exceeded. Control reversal ensued, followed by an inertial roll coupling, a pitchup, and a spin. The X-2 was lost and the pilot killed.

Dick Day was able to recreate on his simulator the full departure of the X-2, including the control reversal, inertial roll coupling, and spin. The X-2 accident had not been prevented, but controllability prediction techniques were learned that would prevent other accidents.

Concurrently with the X-2 flight envelope expansion, Dick became involved in the testing of the Douglas X-3, a jet-powered research airplane designed to accomplish flight research at speeds around Mach 2. The X-3 had short, stubby wings, which meant that it carried most of its mass in its fuselage. During flight test, the airplane experienced two violent roll coupling incidents, wherein the airplane diverged in pitch and yaw during roll maneuvers.

Almost simultaneously with the X-3 divergence, two U.S. Air Force F-100A's, which also contained most of their mass in the fuselage, were lost during flight test due to inertial roll coupling departures. NACA began a series of simulator and flight tests in an attempt to understand roll coupling. An F-100A was flight tested using three vertical tails of different areas and aspect ratios, and a configuration was found that gave the F-100 series of aircraft satisfactory resistance to roll coupling divergence.

The next research program in Dick's career was the X-15 research airplane. Dick's well-rounded engineering talents were never more fully put to use than in the X-15, where he planned the envelope expansion of the airplane with the interim engine (two 8000-lb thrust XLR-11 engines) and then with the production engine (a 60,000-lb thrust XLR-99 engine). He delved into the X-15's stability using the X-15 simulator and discovered a divergent

dutch roll mode at high Mach number. Dick also did mission planning, pilot training, development of operational procedures, and energy management studies.

Dick's work in the X-15 simulator put him in contact with the X-15 pilots, and he passed on to them his knowledge of energy management and of flight with degraded control (for example, damper failures). In a sense, Dick was a flight instructor again, and that was a role he was well-suited to perform. He was patient and articulate, and he had a real depth of knowledge in the subjects that he needed to communicate to the X-15 pilots.

While Dick was making a reputation as a trainer of X-15 pilots, former High Speed Flight Station Director Walt Williams was Director of Operations for Project Mercury at Houston, Texas. Walt had a vacancy in the division responsible for astronaut training, and knew Dick's capabilities from their work together at Edwards. Walt persuaded Dick to take the vacant job, and in February 1962 Dick left Edwards and went to the Project Mercury program as Assistant Division Chief for astronaut training. There, in addition to training astronauts on the simulator, he devised training programs, wrote astronaut tests, and served on the astronaut selection board.

Dick left NASA in 1964 to join the Aerospace Corporation and work on the Manned Orbiting Laboratory. Once again his job was astronaut training. When the Manned Orbiting Laboratory was canceled in 1969, Dick left the Aerospace Corporation and worked in a variety of positions in the aerospace private sector. He worked on diverse test programs that included serving as chief of aerodynamics and flight test engineer on the *Super Pregnant Guppy*, a C-97 aircraft modified to air transport segments of large rocket boosters.

In 1975, the High Speed Flight Station (now renamed the NASA Dryden Flight Research Center) asked Dick to return to work in Space Shuttle simulation. Dick has worked here as civil servant or contract engineer ever since.

Dick has contributed to almost every manned space program in U.S. history. Throughout his career, he has "written the book" on numerous subjects, ranging from rocket aircraft envelope expansion to astronaut training. He has now written the book on coupling dynamics in aircraft. Countless generations of engineers will benefit.

William H. Dana
NASA Dryden Flight Research Center
Edwards, California
November 13, 1996

ACKNOWLEDGMENTS

The author, a former member of, but now retired from NACA/NASA, prepared this report under a contract to NASA Dryden Flight Research Center, Edwards, California. Without the encouragement and support of the following former colleagues and current staff members of Dryden, the text would have resided as a dead file on a floppy disk.

William H. Dana came to NASA High Speed Flight Station on the first day NACA became NASA, October 1, 1958. Today, he is the Chief Engineer, NASA Dryden Flight Research Center, and I wish to thank him for approving the concept and context of this report and advocating its candidacy for publication.

I am also indebted to Kenneth J. Szalai, Director, NASA Dryden Flight Research Center, who read the initial draft, encouraged me to continue the research, and approved publication of this report.

Edwin J. Saltzman arrived at NACA Muroc, California, on July 2, 1951, and still serves NASA in a contractor position. He deserves special thanks for rendering technical advice; serving on the peer technical review committee; locating archival photographs, references, and pertinent publications; and performing the many tasks required to keep the publication process moving.

Robert W. Kempel suggested the title of this report. He also served as a monitor to the progress of the report and gave excellent advice on the sometimes weird manipulations of the equations of motion required for solving flight problems.

Robert G. Hoey was my Air Force counterpart during the X-15 program. He made valuable comments and corrections to early drafts of the X-15 chapter.

Other than my personal recollections, the entire text was assembled from information contained in the list of referenced publications. Material from the following authors was especially helpful:

- William H. Phillips' 1948 NACA Technical Note, describing the theoretical possibility of the occurrence of inertial roll coupling, served as the basis of my attempt to explain this most baffling coupling behavior. As prediction is the true test of theory, some of the X-series research aircraft and Century series fighters did, prophetically, encounter severe inertial roll coupling incidents approximately one-half decade after publication of Phillips' work. Four of these incidents are described in this report.
- Richard P. Hallion's well-thumbed report, NASA SP-4303, *On the Frontier: Flight Research at Dryden, 1946–1981*, has been immensely helpful in providing dates, names, and checks on the accuracy of a considerable portion of the historical material contained in this report.
- Richard D. Banner, Albert E. Kuhl, and Chester H.Wolowicz of NACA and Al Pine of North American Aviation, Inc., Los Angeles, California, contributed significantly. Their pioneering work in deriving new lateral–directional stability equations applicable to the new era of aircraft emerging in the early 1950's proved invaluable to this effort. Because their work is contained in unpublished memorandums, this material is not included in the formal reference list. Instead, the material is listed as footnotes in the text. To my knowledge, this report represents the first time that this unique information has been made publicly available.

I also wish to thank the staff and members of the Dryden Flight Research Center, Research Facilities Directorate for providing the final format of the report and for the expert assistance of the Senior Technical Publications Editor, Camilla F. McArthur. The cover was designed by Steven L. Lighthill.

Richard E. Day

ABSTRACT

Coupling dynamics can produce either adverse or beneficial stability and controllability, depending on the characteristics of the aircraft. This report presents archival anecdotes and analyses of coupling problems experienced by the X-series, Century series, and Space Shuttle aircraft. The three catastrophic sequential coupling modes of the X-2 airplane and the two simultaneous unstable modes of the X-15 and Space Shuttle aircraft are discussed. In addition, the most complex of the coupling interactions, inertia roll coupling, is discussed for the X-2, X-3, F-100A, and YF-102 aircraft. The mechanics of gyroscopics, centrifugal effect, and resonance in coupling dynamics are described. The coupling modes discussed are interacting multiple degrees of freedom of inertial and aerodynamic forces and moments. The aircraft are assumed to be rigid bodies. Structural couplings are not addressed. Various solutions for coupling instabilities are discussed.

INTRODUCTION

This report is not a history of particular aircraft nor of aviation in general. It describes various unique behaviors in aircraft resulting from multiaxis coupling of inertial and aerodynamic parameters. The majority of these phenomena occurred during a period when many important aspects of aircraft technology were developing at an exponential rate. Six classic examples of aircraft that have encountered one or more of four coupling modes are analyzed with anecdotal comments where appropriate. Appendices treat the historical and physical nature of coupling dynamics.

Types of Aircraft Coupling

Following World War II (WWII), aircraft speeds increased through the transonic regime and beyond. With these increases, aircraft began experiencing a series of strange instabilities. Violent motions about all three axes would occur. At times, the severity of these motions resulted in the loss of the aircraft and pilot. These encounters were the result of coupling dynamics that, with the exception of spins, had rarely been experienced previously. Abbreviated definitions of the four coupling modes that were encountered are as follows:

- Inertial roll coupling is a resonant divergence in pitch or yaw when roll rate equals the lower of the pitch or yaw natural frequencies.
- Control coupling is a coupling of static yaw and roll stability and control moments which can produce untrimmability, control reversal, or pilot-induced oscillation (PIO).
- Dutch roll coupling is dynamic lateral–directional stability of the stability axis. This coupling of body axis yaw and roll moments with sideslip can produce lateral–directional instability or PIO. This coupling can also stabilize an aircraft with unstable body axes.
- Spins (steady-state) consist of a stalled, helical descent about a vector spin axis with a balanced coupling of aerodynamic and inertial forces and moments producing constant body and wind axis angular velocities.

Mass properties relative to these coupling modes are listed in appendix A. Other coupling modes, such as roll spiral and translational, are not discussed in this report. Analytical investigation aids, such as classical mechanics as well as analog and digital computers, are presented next. Eras of aircraft evolution are also briefly summarized.

Classical Mechanics

Before WWII and early post-WWII, engineers hand-calculated Euler's equations of motion for criteria to establish operational stability and control boundaries. These calculations were valuable, but the computation

process was extremely slow. Equations of motion for five-degree-of-freedom are shown in appendix B. The following coupling modes did not emerge from these analyses.

Control coupling had not been encountered as a serious controllability problem. As a result, this mode had not been analyzed and set in mathematical form. Discovery of this coupling mode is discussed in the chapters 1 through 3. Relevant equations are developed in appendix C.

Dutch roll was a familiar occurrence. With the fairly conservative lateral–directional stability of the past, dutch roll was, at times, an annoyance, but it was not considered a severe problem. The stability roots of the determinant produced the equation that would later become known as C_{n_β} dynamic. Before the 1950's, this equation did not contain the relevant coupling terms. The historical evolution of the dutch roll equation in this form is developed in appendix D.

Inertial roll coupling had not been "invented" before 1948. Then, William H. Phillips, National Advisory Committee for Aeronautics (NACA), elegantly and cogently described the theoretical possibility of inertial roll coupling occurring.[1] Phillips not only provided the reasons for such couplings but also suggested solutions to the problem should it occur. In the early to mid-1950's, some of the X-series research aircraft and Century series fighters encountered severe inertial roll coupling similar to that which Phillips had foreseen. Phillips' Technical Note almost immediately became a best seller in the aircraft industry and government agencies. Emergence of this problem stimulated a burst of analysis and testing in stability and in control. With help from Phillips' analysis and the emergence of improved electronic computers to guide flight testing, solutions to many coupling problems were soon forthcoming. The fundamental equations for inertial roll coupling are developed in appendix E.

Electronic Computers

The capabilities of electronic computers to solve the differential equations of motion were a substantial improvement over hand calculations. The analog and digital computers were complementary to each other.

Analog Computers

By the early 1950's, analog computers were solving the equations of motion of aircraft in real time. Such computers were sufficiently accurate to permit engineers to model aircraft motions and responses based on wind-tunnel data and on physical characteristics of the aircraft. Incorporating controls and displays allowed operators to close the loop and operate in real time by simulating actual flight. These early simulators were used for engineering analyses, extraction of aerodynamic derivatives from flight data, flight test planning, and pilot indoctrination. The first simulator used for these purposes is discussed in chapter 1. A photo of the simulator is shown as figure 1. The computer-simulator became such a powerful analytical tool that three of the four coupling incidents discussed in this report were discovered either during flight planning or during engineering analysis on simulators. (Inertial roll coupling is the lone exception.) These early analog computer-simulators were the forerunners of modern high-powered, digital computer, entry-to-landing simulators.

Digital Computers

Digital computers were too slow for use in real-time analyses, flight planning, or pilot training in the 1950's. Although extremely accurate, these slow computers were relegated to solving long duration performance problems or short duration stability problems with programmed control inputs. Taking up to 2 hr to make a 6-sec run was quite common.[2]

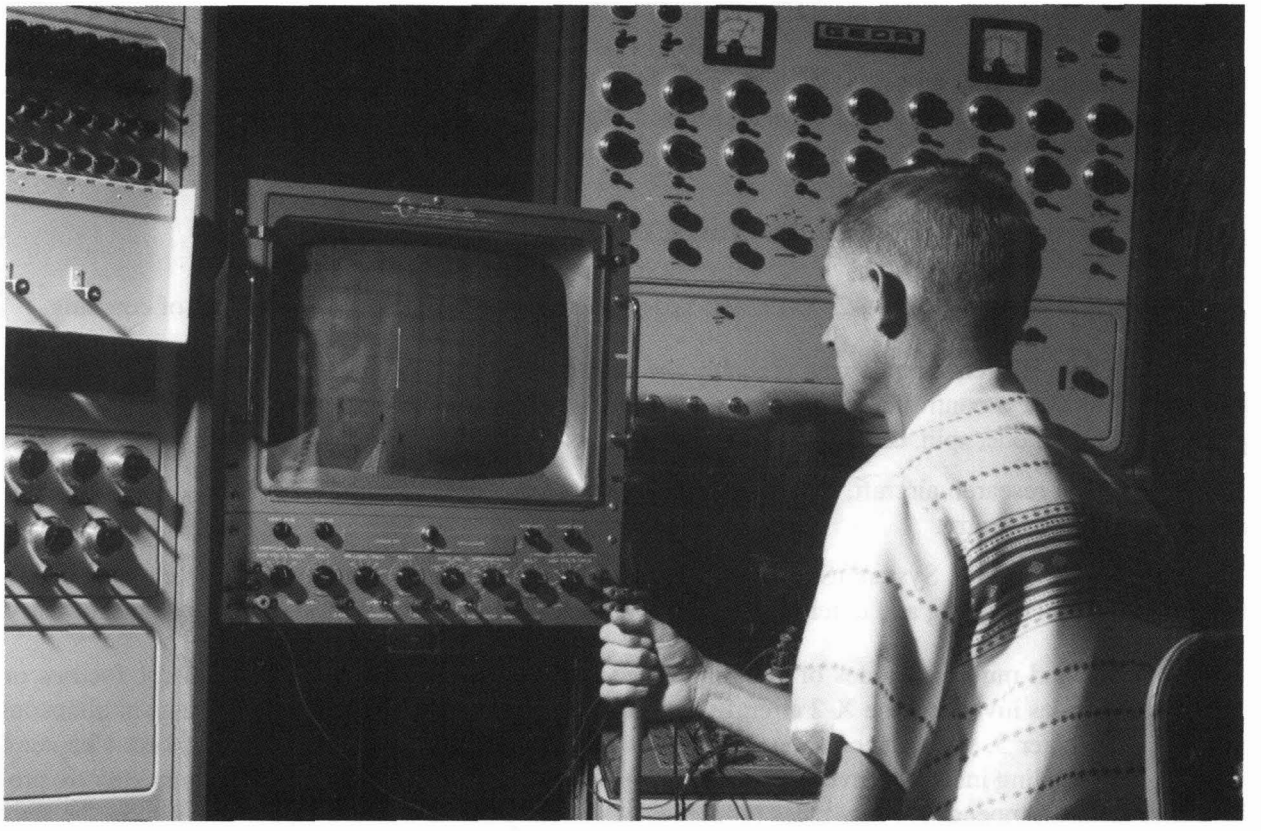

Figure 1. The X-2 five-degree-of-freedom analog simulator arrangement.

Eras of Aircraft Evolution

As measured by increased performance, progress can roughly be ordered in four eras: pre-WWII, WWII, post-WWII, and high tech.

- The pre-WWII era was characterized by low subsonic aerodynamics, transition from wood and linen to metal construction, direct cable-linked controls, and radial engines with moderate power.
- WWII was an era of high subsonic aerodynamics, all metal construction, and in-line, liquid-cooled engines. Cable-linked controls still prevailed.
- The post-WWII era introduced transonic, supersonic, and hypersonic aerodynamics; decreased stability; centerline-loaded inertias; improved metal construction; and boosted irreversible control systems. Other advances included stability augmentation with control damping, superjets, and rocket power.
- The high-tech era introduced entry-to-landing aerodynamics, exotic structural materials, computerized control configured vehicles (CCV), large control surfaces with powerful actuators, fly-by-wire controls, and high thrust-to-weight performance.

Before the end of WWII, except for spins, coupling encounters were not a problem. The rapid advance of technology after the war introduced two factors that greatly enhanced dormant coupling characteristics: large portions of mass concentrated along the centerline of the airplane and performance capability to penetrate the high subsonic, transonic, and supersonic regime where compressibility, turbulent flow, and shock patterns produced highly undesirable stability and control characteristics.

Six classic examples of aircraft that have encountered one or more of the four coupling modes are analyzed in chapters 1 through 4. These aircraft are the X-2 (Bell Aircraft Corporation, Buffalo, New York), X-15 (North American Aviation, Inc., Los Angeles, California), Space Shuttle (Rockwell International, El Segundo, California), X-3 (Douglas Aircraft Company, Santa Monica, California), F-100A (North American Aviation, Los Angeles, California), and YF-102 (Convair, San Diego, California).

Classical Aircraft Coupling Incidents

Three of the aircraft discussed, the X-2, X-15, and Space Shuttle, experienced multiple modes of coupling.

- The X-2 rocket research aircraft was probably the only aircraft to encounter three consecutive coupling incidents. The first, a control coupling mode, led directly to a second mode, inertial roll coupling, which produced a third mode, spin, causing such violent motions that the airplane and pilot were lost.
- The X-15 rocket research aircraft, as designed, encountered decreased dutch roll stability and an unstable control mode during entry.
- The Space Transportation System (STS), or Space Shuttle, had to contend with two unstable modes simultaneously (control coupling and dutch roll coupling) during the hypersonic and supersonic phases of entry.

Each of these aircraft had multiple modes of coupling (each involving control coupling). Chapter 1 focuses on sequential coupling modes involving the X-2 aircraft. Chapter 2 highlights X-15 incidents involving simultaneous coupling modes. In chapter 3, simultaneous coupling modes affecting the Space Shuttle are described. Chapter 4 explores inertial roll coupling incidents involving X-3, F-100A, and YF-102 aircraft. Anecdotal comments are provided where appropriate. Appendix A lists mass properties of coupling-prone aircraft. Appendix B gives the five-degree-of-freedom equations of motion. Appendix C discusses static control coupling. Appendix D discusses dutch roll coupling, and appendix E describes inertial roll coupling.

NOMENCLATURE

Acronyms

ADDB-I	Aerodynamic Design Data Book, first issue
CCV	control configured vehicle
CP	control parameter
GEDA	Goodyear Electronic Differential Analyzer
HSFS	High-Speed Flight Station, Edwards, California
NAA	North American Aviation, Inc., Los Angeles, California
NACA	National Advisory Committee for Aeronautics
NASA	National Aeronautics and Space Administration
PIO	pilot-induced oscillation
RAPP	Research Airplane Projects Panel
RCS	reaction control system
RHC	rotational hand controller
STS	Space Transportation System

Symbols*

a_l	longitudinal acceleration, g units
a_n	normal acceleration, g units
a_t	transverse acceleration, g units
b	wing span, ft
$\bar{c}$	wing mean aerodynamic chord, ft
C_{l_p}	rolling moment coefficient with respect to rolling velocity, per rad/sec
C_{l_r}	rolling moment coefficient with respect to yawing velocity, per rad/sec
C_{l_β}	rolling moment coefficient with respect to sideslip, per deg or per rad
$C_{l_{\delta_a}}$	rolling moment coefficient with respect to aileron deflection, per deg or per rad
$C_{l_{\delta_r}}$	rolling moment coefficient with respect to rudder deflection, per deg
C_{L_α}	lift-curve-slope, per deg
C_{m_q}	pitching moment coefficient with respect to pitching velocity, per rad/sec
C_{m_α}	pitching moment coefficient with respect to angle of attack, per deg
$C_{m_{\delta_e}}$	pitching moment coefficient with respect to elevator deflection, per deg
C_{n_p}	yawing moment coefficient with respect to rolling velocity, per rad/sec
C_{n_r}	yawing moment coefficient with respect to yawing velocity, per rad/sec
C_{n_β}	yawing moment coefficient with respect to sideslip, per deg or per rad
$C_{n_\beta}^*$	dynamic lateral–directional stability of the stability axis, per deg
$C_{n_{\delta_a}}$	yawing moment coefficient with respect to aileron deflection, per deg or per rad
$C_{n_{\delta_r}}$	yawing moment coefficient with respect to rudder deflection, per deg
C_{Y_β}	side force coefficient, per deg
g	acceleration due to gravity, ft/sec^2
h_p	pressure altitude, ft
I_x	roll moment of inertia about body axis, slug-ft^2
I_y	pitch moment of inertia, slug-ft^2
I_z	yaw moment of inertia, slug-ft^2
I_{xz}	roll-yaw cross product of inertia referred to X and Z axes, slug-ft^2

*Dot over a symbol indicates derivative with respect to time.

I_{x_e}	moment of inertia of jet engine rotor, slug-ft^2
i_t	stabilizer deflection, deg
L_v	shear load on vertical tail, lb
L_β	rolling moment with respect to sideslip, per deg
M	Mach number, dimensionless
m	mass, W/g, slugs
N_p	yawing moment with respect to rolling velocity, per rad/sec
N_r	yawing moment with respect to yawing velocity, per rad/sec
N_β	yawing moment with respect to sideslip, per deg
N_β^*	yawing moment of stability axis with respect to sideslip, per deg
N_{δ_a}	yawing moment with respect to aileron deflection, per deg
N_{δ_r}	yawing moment with respect to rudder deflection, per deg
p	body axis rolling velocity, rad/sec
p_0	steady rolling velocity, rad/sec
$\bar{p}$	average roll velocity, rad/sec
q	body axis pitching velocity, rad/sec
$\bar{q}$	dynamic pressure, lb/ft^2
r	body axis yawing velocity, rad/sec
S	wing reference area, ft^2
sec	seconds
t	time, sec
V	true airspeed, ft/sec
W	weight, lb
α	angle of attack of body axis, deg or rad
α_0	initial angle of attack of body axis, deg or rad
α_p	initial angle of attack of principal axis, deg or rad
β	angle of sideslip, deg or rad
$\Delta\alpha$, $\Delta\beta$	increments from initial conditions, deg
δ_a	aileron deflection, (left - right)/2, deg
δ_{a_L}	left aileron deflection, trailing edge down positive, deg
δ_e	elevator deflection, deg
δ_r	rudder deflection, deg
ε	inclination of principal axis, positive when body axis is above principal axis at the nose, deg or rad

θ	angle of pitch relative to flight path direction, rad
ρ	mass density of air, slugs/ft^3
ϕ	bank angle, deg
φ'	bank angle obtained by integrating roll velocity, p, deg
ψ	angle of yaw relative to flight path direction, rad
ω_d	dutch roll frequency, rad/sec
ω_e	rotational velocity of engine rotor, rad/sec
ω_θ	nondimensional ratio of undamped natural frequency in pitch of nonrolling aircraft to steady rolling velocity
ω_Ψ	nondimensional ratio of undamped natural frequency in yaw of nonrolling aircraft to steady rolling velocity

CHAPTER 1
SEQUENTIAL COUPLING MODES
X-2 AIRCRAFT

CONTROL COUPLING → INERTIAL ROLL COUPLING → SPIN COUPLING

During the final Air Force flight, before its scheduled transfer to the NACA, the X-2 airplane became the victim of three distinct coupling modes, one leading directly into the next, eventually destroying the aircraft and killing the pilot. The history and causes of these coupling incidents are described next.

The X-2 airplane was one of a series of experimental research aircraft in the cooperative U.S. Air Force-Navy-NACA High Speed Research program. Two aircraft were built. One was destroyed in 1953. An explosion occurred during captive flight tests, and the airplane was jettisoned over Lake Ontario, New York.

The flight demonstration program of the remaining X-2 airplane was conducted by the U.S. Air Force at Edwards Air Force Base, California. The NACA High Speed Flight Station (HSFS) provided engineering support. The U.S. Air Force provided the B-50 mothership (carrier), cockpit camera, and pilots. Bell Aircraft Corporation provided operational support and trajectory calculations. The NACA HSFS provided standard stability and control recording instrumentation, radar tracking, stability and control analysis, and simulator programming and operation. The author was assigned as the NACA project engineer in 1953.

Figure 2 shows the X-2 airplane. The X-2 was air-launched, rocket-powered and landed on the playa surface at Muroc Dry Lake on an extendible skid landing gear. Appendix A lists the mass properties and various inertia ratios affecting coupling characteristics of the X-2 and five other aircraft. Lt. Col. Pete Everest was the project pilot, and Capt. Iven C. Kincheloe was assigned to altitude flights. Capt. Milburn G. Apt was assigned to speed flights following Everest's military reassignment in 1956. The airplane was scheduled to be turned over to the NACA after powered flight 13. After the transfer, NACA plans included installing aerodynamic heating instrumentation. Unfortunately, this transfer did not occur. On the final flight, powered flight 13, the airplane and pilot were lost because of coupling incidents described below.

One of the highlights of this alliance was that, on recommendation of the NACA, the Air Force obtained a Goodyear Electronic Differential Analyzer (GEDA) analog computer. At about this time, the electronic analog computer was coming into its own as a device for solving highly complex, nonlinear, differential equations with an adequate degree of accuracy for piloted closed-loop stability and control analyses.

Figure 1 shows portions of the computer and simulator arrangement. NACA engineers provided the five-degree-of-freedom equations of motion (appendix B), aerodynamic derivatives, and displays and controls for the analog computer to develop the X-2 simulator. NACA engineers also provided X-2 simulator operations and pilot briefings. Incidentally, this was the first simulator used (1954) for the combined functions of flight test planning, pilot training, aerodynamic derivative extraction, and analysis of flight data.

FLIGHT TEST PROGRESS

Progress of the flight test program had been extremely slow, but the X-2 finally managed to get to the higher altitudes and Mach numbers. During a June 1956 joint NACA, Air Force, and Bell Aircraft meeting, the Air Force agreed to deliver the X-2 to NACA by October 1, 1956.[3] By this time, the X-2 had attained Mach 2.53. On July 23, 1956, the X-2 achieved Mach 2.87 during the ninth powered flight. On September 7, 1956, the Air Force had completed its twelfth powered flight (Kincheloe's flight to 126,200 ft) and scheduled one more flight to reach the design speed of Mach 3 before delivery to the NACA by October 1.

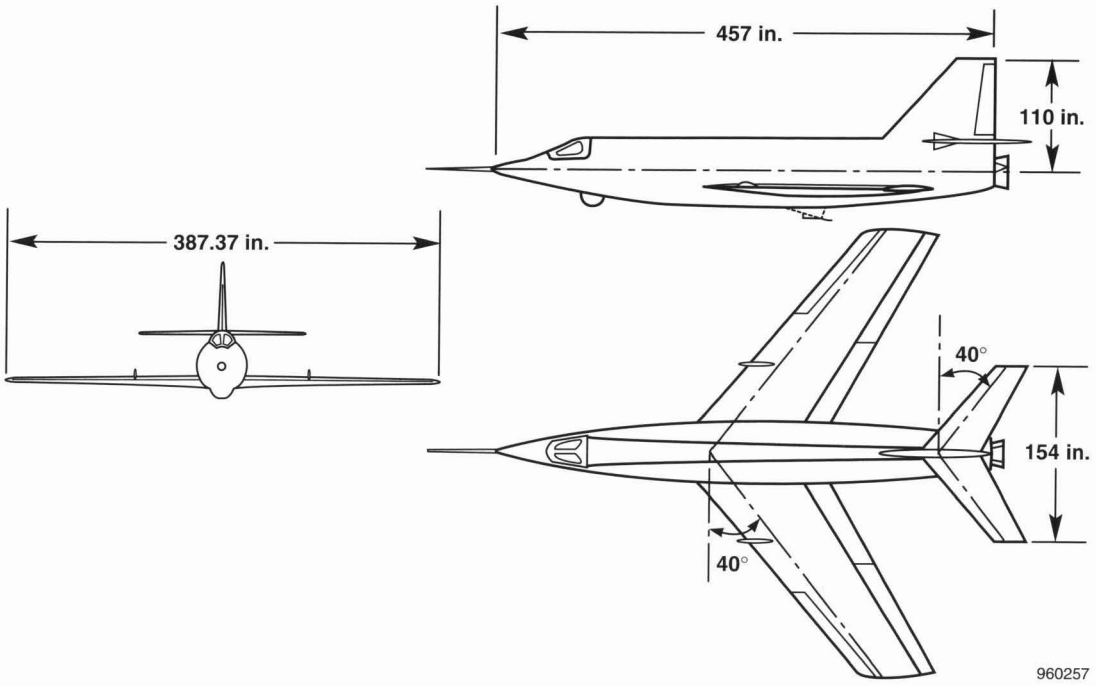

(a) Three-view drawing.

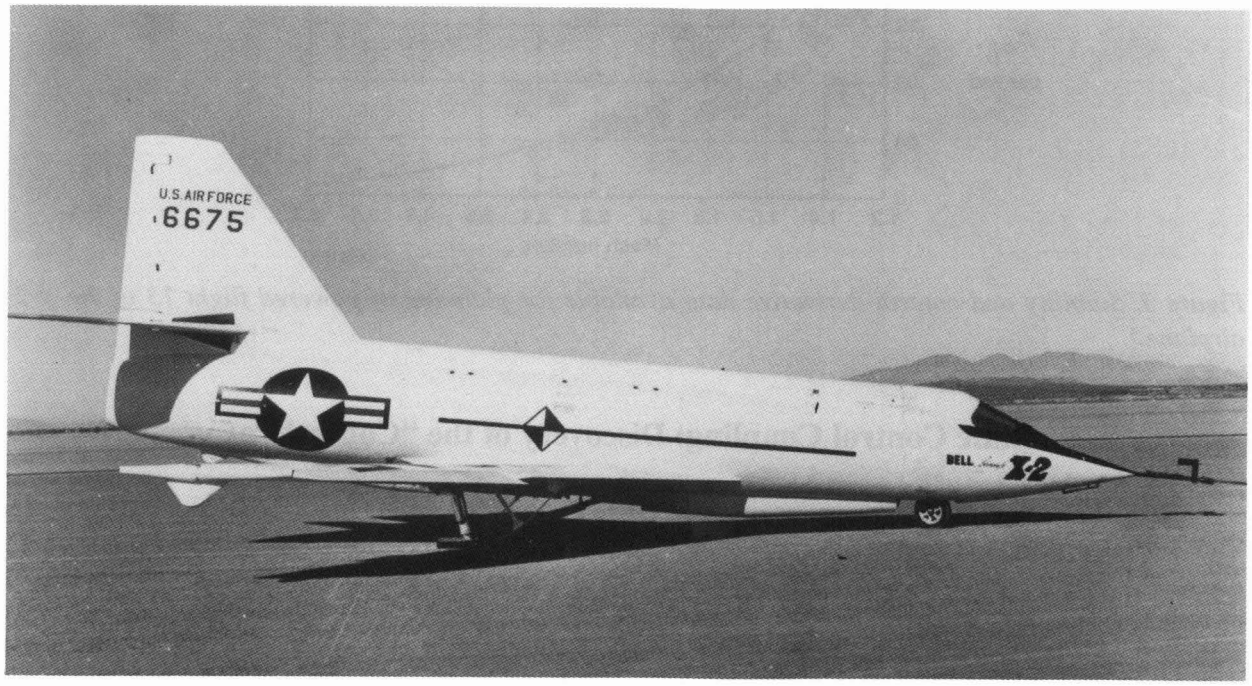

E-2817

(b) Photograph.

Figure 2. Three-view drawing and photograph of the X-2 rocket research airplane.

On each flight, NACA engineers requested that the pilots perform longitudinal and lateral control pulses for aerodynamic derivative extraction. The magnitude and execution of the pulses were practiced on the simulator before flight. In-flight control pulses were not performed beyond Mach 2.4. Consequently, stability and control flight data extended only to Mach 2.4 (fig. 3).[4] These stability and control data were at a dangerously low value

and, according to theory, should continue to decrease with increasing Mach number. At this point, Everest received a military reassignment, and Capt. Apt was designated as the X-2 pilot.

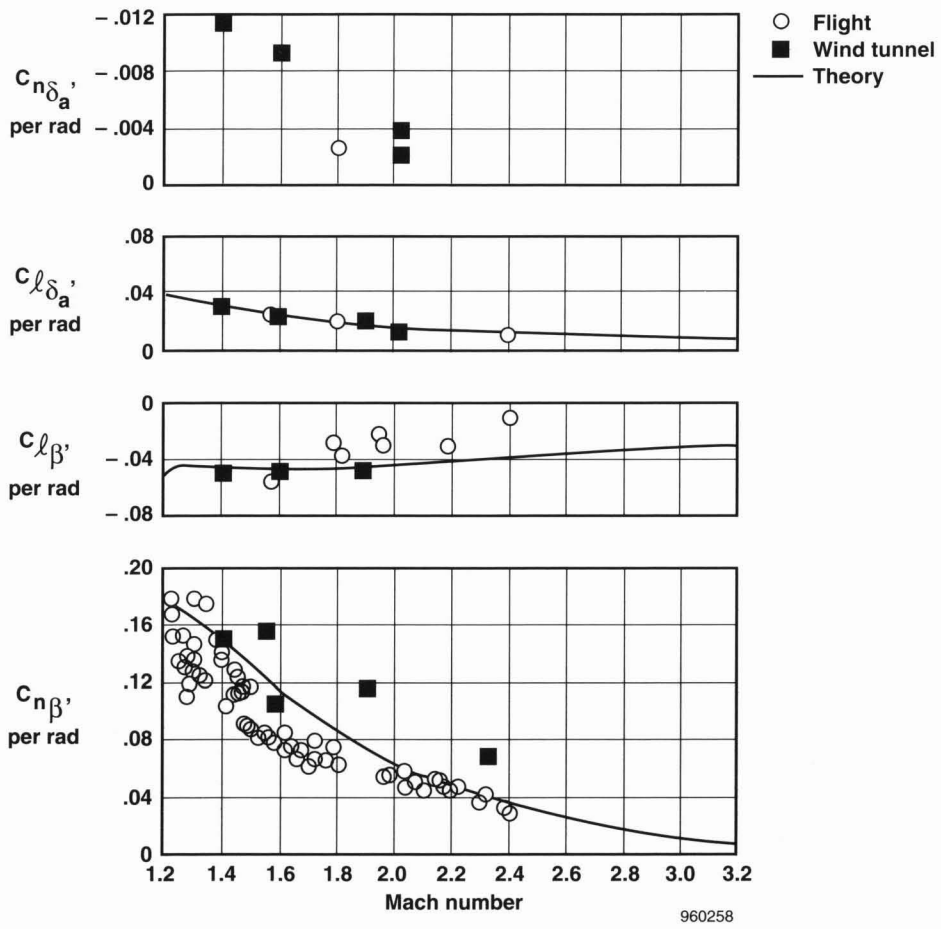

Figure 3. Stability and control derivative data available for planning of powered flight 13 of the X-2 research airplane.[4]

Static Control Coupling: Discovery of the "Control Parameter"

During a flight planning session, *prior* to the powered flight program, control coupling was first encountered. The simulator was programmed for Mach 3 with stability and control coefficients obtained from wind-tunnel data and theory. While flying the simulator, any attempt to bank or roll the aircraft resulted in the wings remaining level or rolling in the opposite direction, leading to violent uncontrollable motions. These violent motions had a familiar signature and were immediately recognized as those of inertial roll coupling; however, the adverse control condition leading to the coupling had not been experienced previously. Hubert Drake, NACA HSFS Director of Research, was observing and suggested that the probable cause for the slow divergence was adverse aileron producing adverse yaw such that the effective dihedral (roll due to yaw) was balancing or even opposing rolling moment. The rudder was locked on the X-2 for supersonic flight leaving only aileron for lateral–directional control. The balance equation, $C_{n_\beta}/C_{n_{\delta_a}} = C_{l_\beta}/C_{l_{\delta_a}}$, was then used to monitor and predict this type of instability (appendix C).

Because this phenomenon had not previously been encountered, no identifying label, such as inertial coupling or dutch roll, existed. The phenomenon was simply referred to as the control parameter. Eighteen years later, Rockwell engineers using wind-tunnel data rediscovered that this instability would occur during the Space Shuttle

entry and solved the problem by use of reaction rockets and a sophisticated computer control system; neither of which was available during the X-2 program. Chapter 3 provides a detailed analysis of the Space Shuttle control coupling instability and how it was overcome.

It is interesting to note that one type of rather calm, slowly developing, coupling instability (control coupling) led to the onset of another, rapidly developing, coupling instability (inertial roll coupling) exhibiting violent uncontrollable motions which in turn produced a third coupling mode, supersonic spin.

Many runs were made on the simulator by the X-2 pilots to demonstrate this unsafe area and how to recover from control coupling if motions were beginning to diverge (a pushover to near zero *g*). Pilots were instructed to maintain low angles of attack until slowing to Mach 2.4 at which speed it was safe to increase load factor (angle of attack) for turns. Everest was apparently sufficiently convinced that on his record-breaking flight of July 23, 1956, he decelerated from Mach 2.87 to Mach 2.2 before entering a turn to return safely to Muroc Dry Lake.[4] Everest, however, was not painted into a corner as was Apt. Apt's dilemma is discussed below.

PREDESTINED DOOM

Many stories are told of aircraft that encounter a series of events that eventually lead to the demise of the aircraft, for example hot day, short runway, and low power. The final and record-breaking flight of the X-2 on September 27, 1956, was such an example. Cumulative events that contributed to the fatal incident are listed below:

- Optimum energy boost trajectory.
- The rocket burn was longer than predicted by 15 sec and positioned the pilot further from Muroc Dry Lake than expected.
- Decrease in directional stability as speed increased.
- Decrease in directional stability with increased lift, leading to a reduced critical roll rate for inertial coupling.
- Adverse aileron control (control reversal).
- High positive effective dihedral.
- Rudder locked supersonically.
- Mass properties in "window of susceptibility" for inertial roll coupling.

These combined effects culminated in a supersonic spin and an eventual subsonic inverted spin.

Some considered Apt's inexperience in flying rocket aircraft as a possible contributing factor to the fatal incident. Perhaps this factor should not be considered because Capt. Apt flew the rocket-powered portion of the flight without difficulty and exactly as prescribed. He had also flown many roll coupling tests in the F-100A but none as insidious as powered flight 13. It was only after rocket burnout that a crucial decision had to be made.

Scenario of Final Flight

Apt had flown the simulator and received briefings on July 29, 1956. He also had several unlogged, informal simulator sessions between that date and September 24 to prepare for powered flight 13 on September 27. These practice sessions included maneuvers at several Mach numbers up to Mach 3. During these sessions, recovery methods applicable to control coupling were practiced.

The scenario of events on the final flight that led to the catastrophic end is as follows: Apt had flown an optimum performance trajectory, and the rocket had burned to propellant depletion, longer than had been predicted.

This unexpected increase in performance (Mach 3.2) positioned him farther from the Muroc Dry Lake landing site than anticipated. At this point, Apt literally was trapped. He had to decide whether to decelerate through Mach 2.4, as briefed, in order to make a safe turn, or to make the turn immediately. The first option, decelerating, would have increased the distance from the desired landing site even farther. The second option involved risking the instabilities that had been predicted and "flown" during simulator practice runs. The simulator was new and had never been used previously as a flight planning tool. Most pilots had, in fact, expressed a certain amount of distrust. Whether distrust of the simulator or a fear of not making it back to Muroc Dry Lake affected the decision, he opted for the turn.

Control Coupling

The X-2 remained stable up to Mach 3.2 while at low angles of attack. After burnout (158 sec, fig. 4), however, control motions were initiated to increase the angle of attack and to produce a left bank (160 sec). As the speed decreased below Mach 3 and the angle of attack simultaneously increased, the directional stability was lowered to such an extent (fig. 5) that when corrective aileron was applied to stop the increasing left bank angle (caused by dihedral effect), the yawing moment resulting from the aileron deflection exceeded the restoring moment caused by sideslip. In addition, the roll due to sideslip exceeded the maximum capabilities of the ailerons.

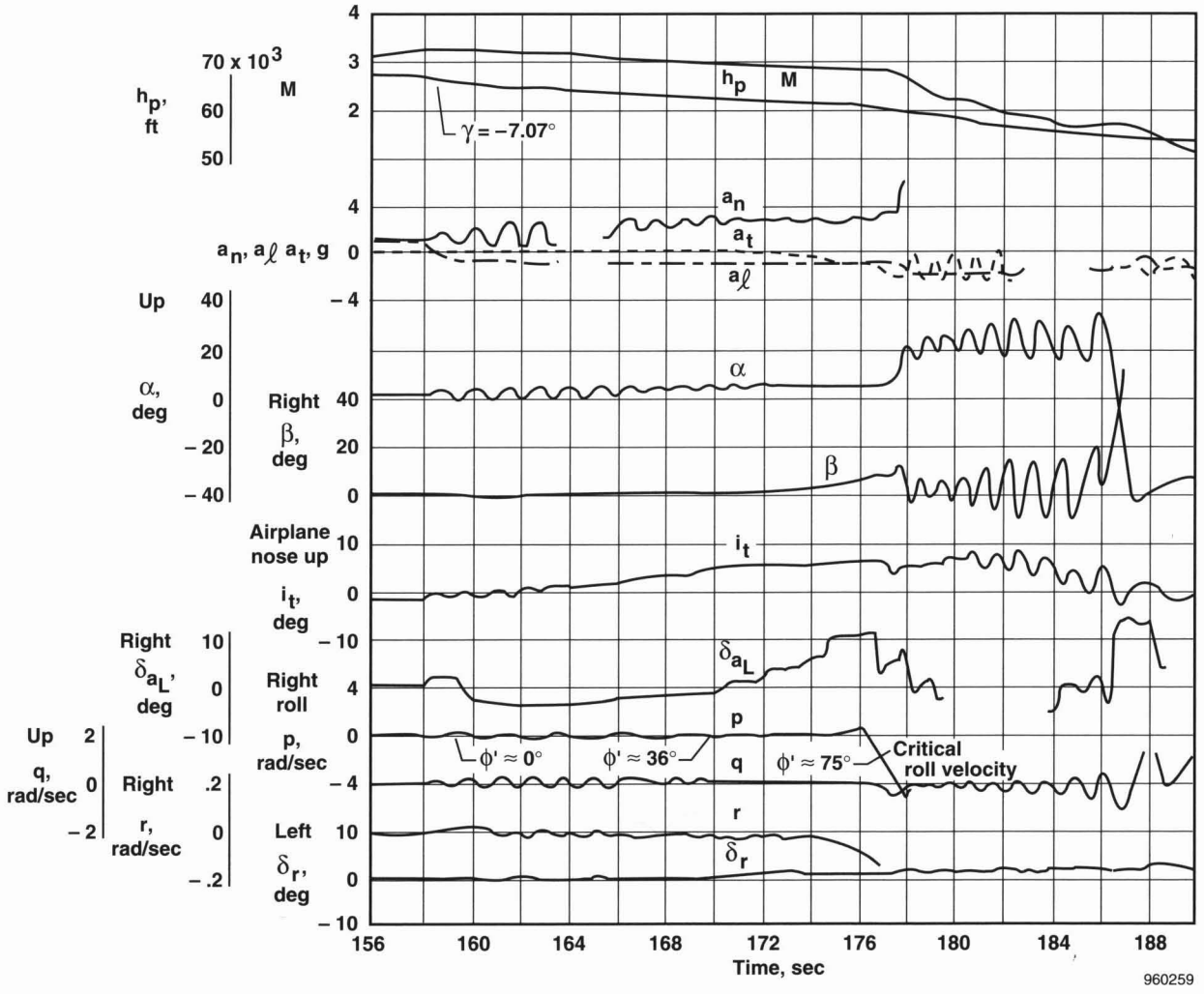

Figure 4. Time history of powered flight 13 of the X-2 showing directional divergence. Gaps in record resulted from exposure to daylight.[4]

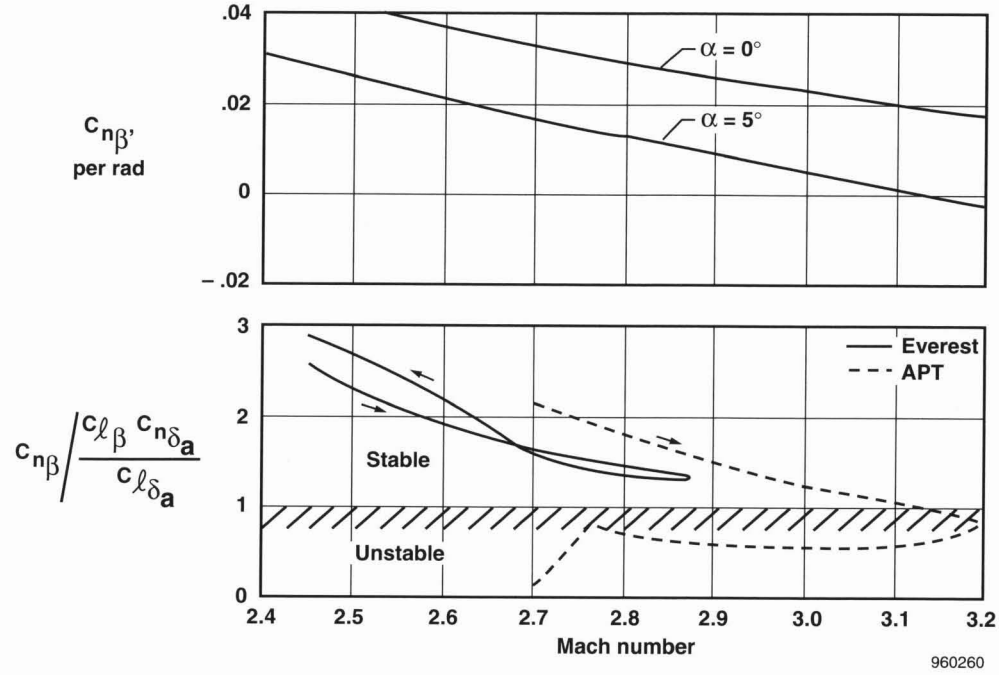

Figure 5. Directional-stability data of high Mach number X-2 flights using wind tunnel derivatives for flight conditions.[4]

As described above and developed in appendix C, neutral lateral control can be expressed for the rudder locked by the control parameter,

$$C_{n_\beta} / C_{n_{\delta_a}} = C_{l_\beta} / C_{l_{\delta_a}}$$

Rearranging the equation as it is shown in figure 5,

$$C_{n_\beta} \Big/ \frac{C_{l_\beta} C_{n_{\delta_a}}}{C_{l_{\delta_a}}} = 1$$

indicates that the control parameter must be greater than one for proverse control. The directional stability coefficient of the X-2 was positive at all times (fig. 5). However, the increase in angle of attack lowered C_{n_β} below the critical value, allowing inputs to initiate the divergence. Figure 5 shows the control parameter (based on flight angles of attack and Mach numbers) for Everest's and Apt's flights before and after burnout and near the peak Mach numbers. Although a portion of Everest's flight was in the Mach number range where an instability could occur, Everest maintained a low angle of attack down to Mach 2.2, keeping C_{n_β} greater than the critical value for control coupling.[4] His flight was within the acceptable parameters he had received during the briefings and simulator practice runs.

INERTIAL ROLL COUPLING[†]

After burnout at 158 sec, longitudinal oscillations of ±1° occurred (fig. 4). These oscillations were probably caused by longitudinal rocket thrust misalignment. The pilot attempted to damp the vertical oscillations and approximately 1 sec later initiated a left turn gradually increasing airplane nose up stabilizer, i_t, increasing the angle of attack to 5° and aileron to neutral at 170 sec. From time 170 to 177 sec, the pilot applied right aileron, but the airplane continued to roll left. At 5° angle of attack, the reduced directional stability decreased the control parameter (fig. 5) such that sideslip gradually diverged from zero to plus 8° at 177 sec.

These motions continued to increase until critical roll velocity for inertial coupling (calculated to be 1.35 rad/sec for these conditions) was exceeded at 177 sec. At critical roll velocity, violent uncontrollable motions characteristic of inertial roll coupling occurred about all three axes.

Supersonic Upright to Subsonic Inverted Spin

Near time 178 sec, the diverging sideslip suddenly returned to and oscillated about zero. At the same time, the angle of attack pitched to 20°, and the airplane entered into an erect accelerated supersonic spin. The erect spin was maintained for 8 sec until, at time 186 sec, the aircraft suddenly pitched down 70° from an angle of attack of 30° to –40° and entered into an inverted spin. Two seconds later, the aircraft went subsonic. It is interesting to note that inertial roll coupling served as a catalyst in going from adverse control coupling to a supersonic, upright, accelerated spin in a period of approximately 1 sec.

Observing the timeline of the various coupling modes shown in figure 4 reveals approximately 17 sec of adverse control coupling from time 160 to 177 sec, 1 sec of inertial roll coupling from time 177 to 178 sec, and, as noted above, 8 sec of supersonic spin from time 178 to 186 sec. The cockpit camera indicated that the pilot made two recovery attempts. Then, he ejected the nose capsule ($t \sim 220$ sec) at a subsonic Mach number and an altitude of approximately 40,000 ft. The separation was clean, and the deceleration-stabilization parachute deployed and trailed properly, but the pilot could not effect a separation from the capsule and was killed on impact. The airplane had sustained minimal damage when it landed unmanned in the desert.

Records Recovered

The NACA data recorders were recovered, and the film developed clearly except for fogging near the end as indicated in figure 4. When the film was delivered from the photography laboratory and unrolled to view, it was déjà-vu. The film traces looked exactly like the recorder traces of simulator runs and, in particular, the training runs made before the flight. It was immediately apparent what the gruesome series of events were, how they happened, and why they happened.

The cockpit camera was also recovered. This camera was used to correlate certain events with the internal NACA recorders.

ADDITIONAL COMMENTS REGARDING THE X-2 INCIDENT

Attempted Restoration of Data Records

The NACA instrumentation stopped recording when the capsule ejection interrupted power and certain areas were light struck as a result of the crash (fig. 4). After the film had been copied, it was sent to the Federal Bureau of

[†]Inertial roll coupling is discussed in this chapter because it is one of three modes occurring on one flight. Chapter 4 is devoted to inertial roll coupling and discusses inertial roll coupling incidents of three other aircraft. The physics and math implications of inertial roll coupling are described in appendix E.

Investigation to see if any of the light struck areas of the film could be restored. Unfortunately, these data were beyond rescue.

X-2 Accident Investigation Board

Following the X-2 accident, this author was appointed to the accident investigation board to analyze and prepare the aerodynamic (stability and control) section of the accident report. This section of the accident report was somewhat similar to the above description but also included copies of (strip recorder) simulator runs made by Apt prior to the flight. As an addition to the report, an animated film using an X-2 model demonstrated the violent motions that are shown in figure 4.

Reaction Control Studies

During this time, NACA was also using the GEDA analog computer to study handling quality requirements for reaction controls at extremely low or nonexistent dynamic pressure. Although the X-2 airplane flew at dynamic pressures as low as 19 lb/ft^2 during Iven Kincheloe's high-altitude flight,[4] the application of a reaction control system (RCS) to the airplane was not studied on the simulator. During the final flight, the X-2 was at a relatively high dynamic pressure (840 lb/ft^2 at the onset of control instability and 770 lb/ft^2 at roll coupling divergence). One would not think that RCS would help at these high dynamic pressures. However, the directional stability was so low at the increased angle of attack that current computer runs indicate that yaw reaction jets of less than 5-lb thrust would have restored controllability.

Proposal to Salvage the X-2 and Modify to Hypersonic Configuration

"In committee meetings in 1951 and 1952, Robert Woods (Bell Aircraft Corporation) recommended that the NACA study requirements for hypersonic ($M > 5$) manned flight...Langley engineers proposed salvaging the X-2 for a hypersonic test program using two jettisonable rockets and adding reaction controls."[3] (The X-2 had landed unmanned in the desert, minus the cockpit capsule, with little damage.) The X-2 was unfortunately in the twilight zone of progress where rocket power, structural integrity, and thermodynamics were sufficiently advanced to push the aircraft to supersonic speeds. However, hydraulic controls and computerized control augmentation systems were not yet developed enough to contend with the instabilities. The X-2 airplane was not approved for the modification.

CHAPTER 2
SIMULTANEOUS COUPLING MODES X-15 AIRCRAFT

DUTCH ROLL COUPLING → CONTROL COUPLING

Chapter 1 described three X-2 coupling modes. Each was unstable, one mode leading directly to another with disastrous results. During X-15 entries or during supersonic flight at moderate angles of attack, two coupling modes occurred with the dutch roll mode contributing to an unstable control mode.

Although the demise of the X-2 prevented NACA from obtaining anticipated high supersonic heating data, postflight examination at the crash scene indicated that although the aircraft had sustained a period of 15 sec above Mach 3, the stainless steel skin had not suffered from aerodynamic heating. This finding indicated that the time had come to expand the experimental research program into the hypersonic speed regime. The need for such expansion had been recognized some years earlier. In 1952, the NACA Committee on Aeronautics urged that NACA study requirements for piloted hypersonic aircraft. After many meetings and much discussion, the X-15 was approved. In June 1956, North American Aviation, Inc. (Los Angeles, California), was awarded a contract for three X-15 aircraft.[5] Reaction Motors, Inc. (Rockaway, New Jersey), was given a contract to develop the XLR-99 rocket engine. By September 1956, enough wind-tunnel and structural data had been collected so that construction of the first X-15 could be started. The X-15 was the only X-series aircraft that was designed for, and would fly to, hypersonic speeds and extreme altitudes. It was the most successful of the X-series aircraft, especially in returning research data for future design criteria. The three X-15s flew 199 flights from June 1959 to October 1968.[6] Figure 6 shows the X-15 aircraft. Coupling inertia ratios for various aircraft are shown in appendix A.

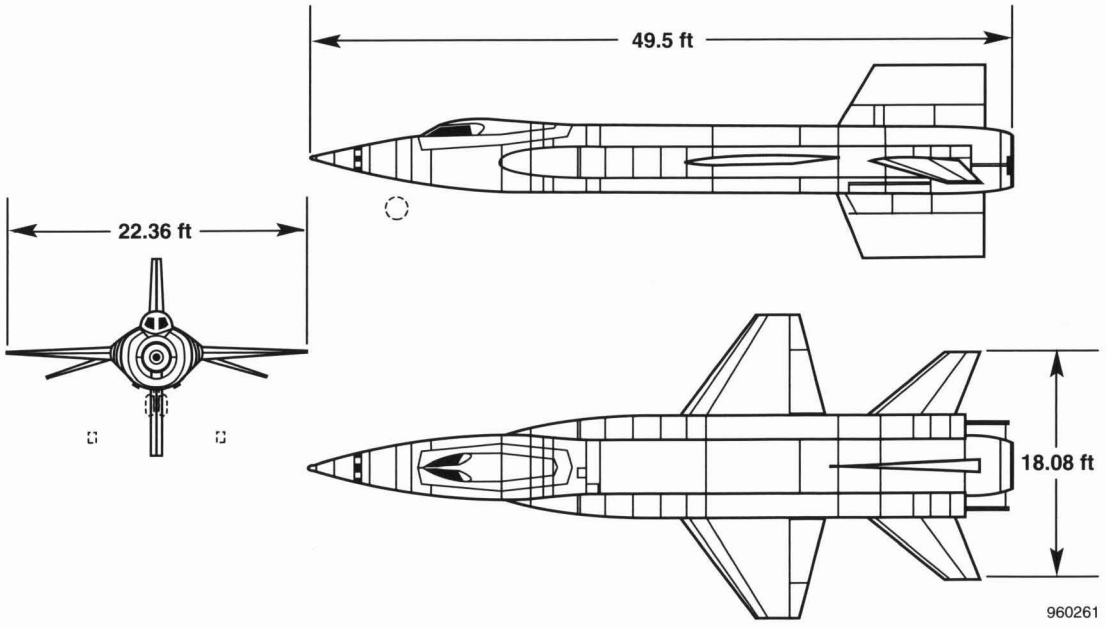

(a) Three-view drawing.

Figure 6. Three-view drawing and photograph of the X-15 research airplane.

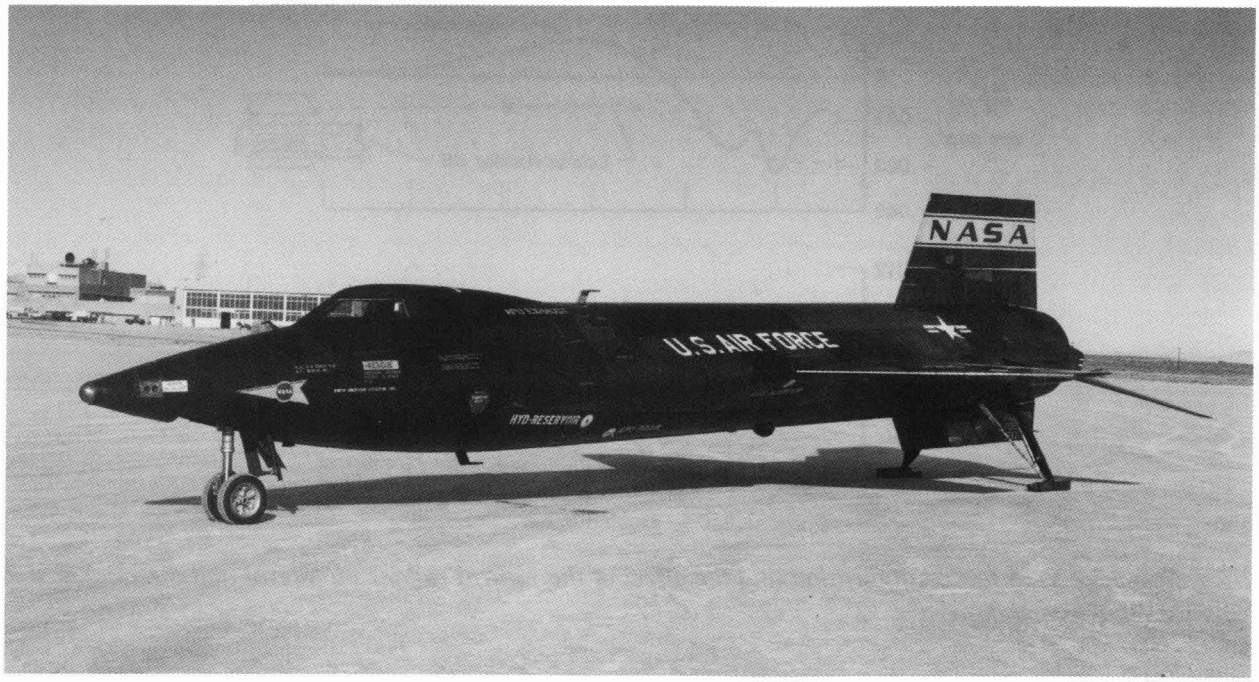

(b) Photograph. (Courtesy of the U.S. Air Force.)

Figure 6. Concluded.

DUTCH ROLL COUPLING

The following is a short definition of the dutch roll mode: dynamic lateral–directional stability of the stability axis. This coupling of body axis yaw and roll moments with sideslip can produce lateral–directional instability *or* stabilize an aircraft with unstable body axes. The dutch roll equation (developed in appendix D) is

$$C_{n_\beta}^{*} = C_{n_\beta}\cos\alpha_0 - I_z/I_x C_{l_\beta}\sin\alpha_0$$

Although the stick-fixed dutch roll stability is positive above Mach 2.3 in some areas of the X-15 flight envelope, effective dihedral becomes adverse and introduces control divergence. This control divergence is discussed in the Dynamic Control Coupling section of this chapter.

The X-15 is a good example of the impact of dutch roll coupling on handling qualities. The X-15, as designed, was adversely affected, not benefited by dutch roll. However, serendipity came to the rescue, and a rather simple modification altered dutch roll characteristics such that controllable entries could be flown from X-15 altitude flights.

During the design phase of the X-15, engineers were concerned that a fairly large potential thrust misalignment would require substantial directional stability and rudder power to hold the nose straight during the exit phase just before burnout at low dynamic pressure. To overcome this potential deficiency, the design engineers added a ventral stabilizer and a jettisonable (for landing) all-movable rudder mirroring the dorsal stabilizer and rudder. Figure 7 shows a sketch of the X-15 airplane with the lower rudder on and off.[7,8] As the flight program proceeded, thrust misalignment did not materialize, but the added ventral that was intended to solve one control problem produced another, not during powered flight but after burnout at the higher angles of attack required for entry from high-altitude flights.

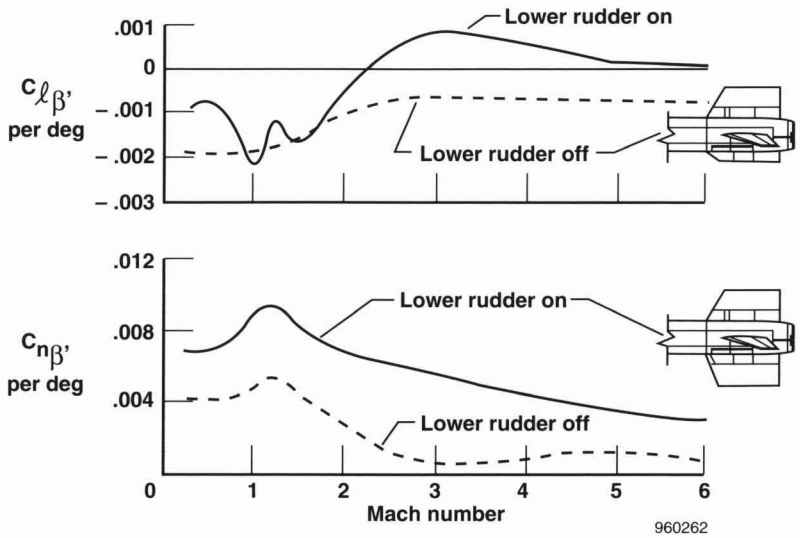

Figure 7. Sketch of X-15 tail configuration and the effect of the ventral rudder on lateral and directional stability derivatives. Wind tunnel data, $\alpha = 12°$.[7]

DYNAMIC CONTROL COUPLING

Supersonic lateral–directional control was provided by differential deflection of the all-movable horizontal stabilizers, referred to as the "rolling tail." The rudder was not used for directional control at the higher speeds and during entry. Figure 7 shows the values of C_{n_β} and C_{l_β} with Mach number at an angle of attack of 12° with ventral rudder on and off. This trend exists for angles of attack above approximately 5°. At high angle of attack, the ventral is more effective than the dorsal, and being below the roll axis gives an adverse roll with sideslip. This is shown in figure 7 as effective dihedral changes from stable ($-C_{l_\beta}$) to unstable ($+C_{l_\beta}$) beyond Mach 2.3, and although dutch roll stability (C_{n_β}*) remains stable, the adverse roll-to-sideslip ($+C_{l_\beta}$) introduces the controllability problem. When the pilot is controlling in the conventional mode by applying roll control proportional to and opposite to bank angle ($-\delta_a \sim \phi$) and effective dihedral is unstable ($+C_{l_\beta}$), the pilot-airplane loop becomes dynamically unstable, and the pilot is actually feeding or increasing the amplitude of sideslip with each cycle. This effect is shown in figures 8, 9, and 10[7,8] as lateral–directional dynamic divergence when the pilot attempts to control with aileron proportional to and opposing bank angle.[9]

The time history shown in figure 8 indicates that diverging lateral–directional motions subside when the angle of attack is reduced. Reducing the initial angle of attack, α_0, minimizes the powerful effect of the inertia ratio ($I_z/I_x = 24$)[‡] and also the adverse dihedral ($+C_{l_\beta}$) which became more unstable with increasing angle of attack. C_{l_β} was also a strong function of angle of attack. As the angle of attack increased, the compression field under the fuselage increased the effectiveness of the ventral while the expansion field above the fuselage reduced the effectiveness of the dorsal such that C_{l_β} became more positive (unstable) with increasing angle of attack. The product

[‡]Yaw to roll inertia ratios for six aircraft.

Aircraft	X-15	X-3	Shuttle	YF-102	F-100A	X-2
I_z/I_x	24.0	15.9	8.0	8.7	5.9	5.8

of these components appears in the second term of the dutch roll equation. In the latter half of the time history as angle of attack is increased, the motions again diverge. This time history is from an X-15 flight during deceleration from Mach 3 to approximately Mach 2.

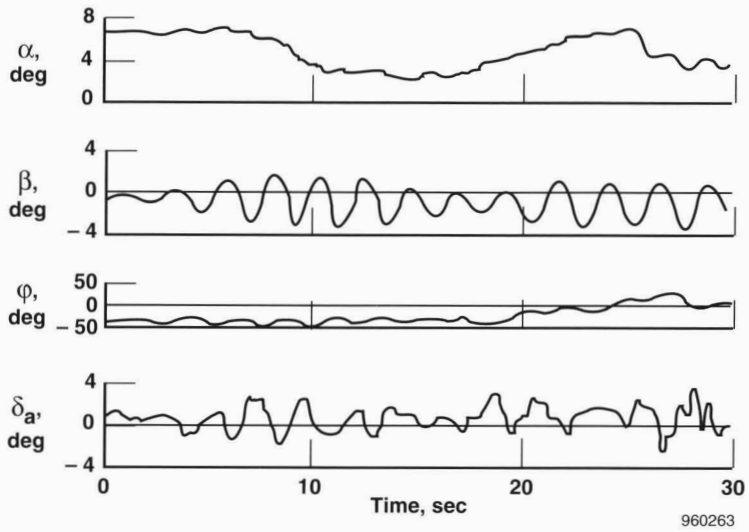

Figure 8. Effect of angle of attack on X-15 controllability. X-15 during-flight. Roll dampers off. Center stick.[7,8]

Figure 9 shows a time history from the F-100C variable stability airplane. In the first part of this time history, the pilot attempted to hold the stick fixed, but inadvertent lateral control inputs resulted in divergent oscillations. During the center portion of the time history, the pilot released the stick and the motions damped, indicating that dutch roll was still stable although effective dihedral was adverse. In the last part, the pilot attempted to control in the conventional manner, and the motions again diverged.

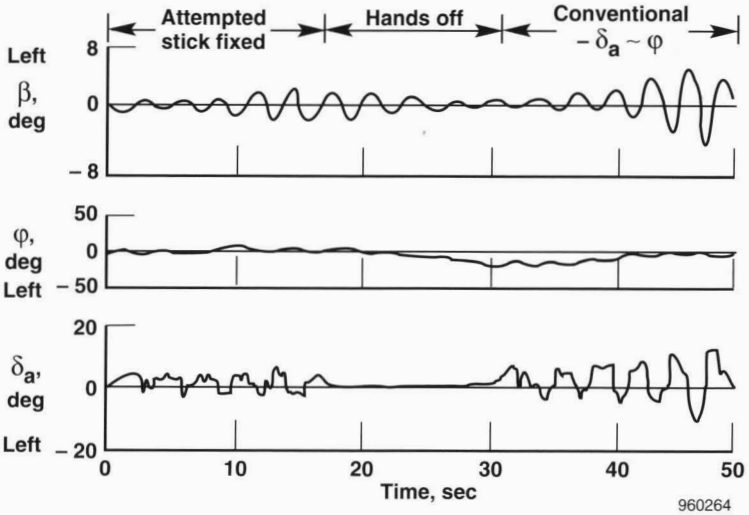

Figure 9. Effect of pilot on controllability. F-100C variable-stability airplane.[7,8]

The time history of figure 10 was obtained with the pilot "flying" the X-15 six-degree-of-freedom simulator using the $\dot{\beta}$ control technique. Development of the betadot, $\dot{\beta}$, control technique is discussed later in this chapter. The first part of the time history shows sideslip diverging as the pilot applies conventional control. During the second part of the time history, the pilot quickly damps the divergent oscillations with sharp lateral pulses opposing the direction of the sideslip needle as it swings through zero (when the rate of change of sideslip, $\dot{\beta}$, is maximum).

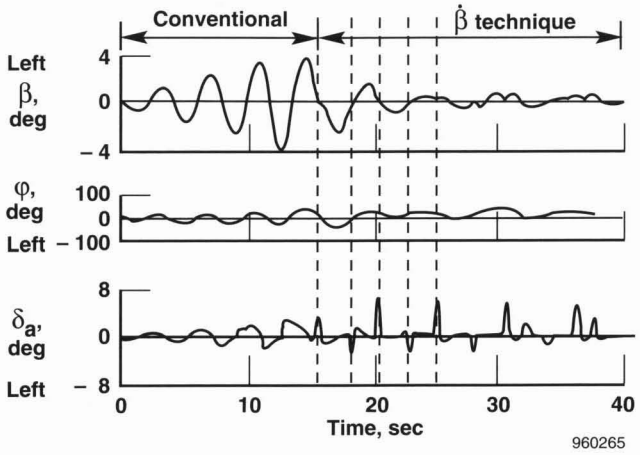

Figure 10. Illustration of $\dot{\beta}$ control technique. Fixed base X-15 simulator.

This control coupling problem was not realized until this author was well into planning for the high-altitude entries using the North American X-15 six-degree-of-freedom analog simulator (fig. 11). As the planning continued to higher altitudes, approximately 200,000 ft and above, the required angles of attack for entry produced marginal controllability with the rate dampers engaged and total uncontrollability with dampers failed.

During previous programs, NACA flight planners had worked frequently with the dutch roll equation to extract aerodynamic derivatives from flight data control pulses (appendix D). Recalling the members of the terms in the equation,

$$C_{n_\beta}^{\ *} = C_{n_\beta}\cos\alpha_0 - I_z/I_x C_{l_\beta}\sin\alpha_0$$

it suddenly became obvious that with positive C_{l_β}, conventional control using aileron proportional to and opposing bank angle would produce a control divergence.

A review of the wind-tunnel data indicated that the positive C_{l_β} was sufficiently high to confirm that the source of the adverse roll was the location of the ventral below the roll axis. To test this hypothesis, the positive C_{l_β} slope being used in the simulator was replaced by an assumed negative slope that would represent the removal of the ventral rudder leaving only the stubby stabilizer. This somewhat simple solution worked fine for simulator runs. Later, limited ventral off wind-tunnel data were used. The combination of the new and favorable derivatives permitted simulator dampers-off controllable entries. The next step was to validate that the trends indicated in the sparse wind-tunnel data were valid in flight. The first ventral-off flight was flown on October 4, 1961, by Capt. Robert Rushworth. This was a short flight to only Mach 4.3, but these data confirmed that the directional stability was adequate and that C_{l_β} was negative, as expected. During the subsequent 11 months, sufficient additional wind-tunnel data were obtained in the ventral-off configuration to round out the aerodynamic predictions and to

convince management that the configuration provided a safety improvement over the ventral-on configuration. All 130 flights following flight 69 on September 28, 1962, were made with the ventral-off.

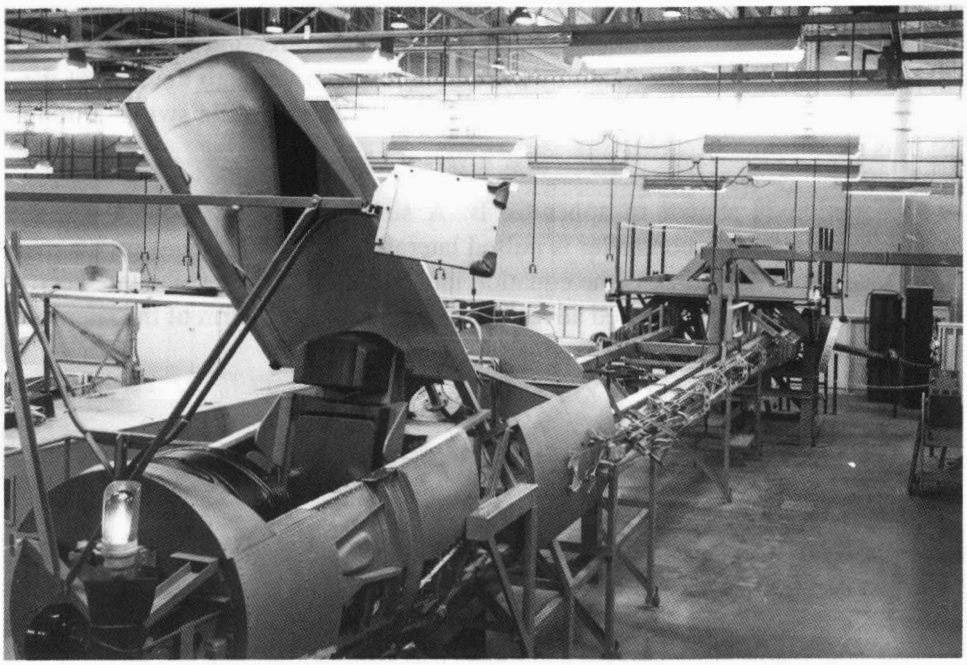

(a) Cockpit controls, display panel, and integrated control system hardware test bed.

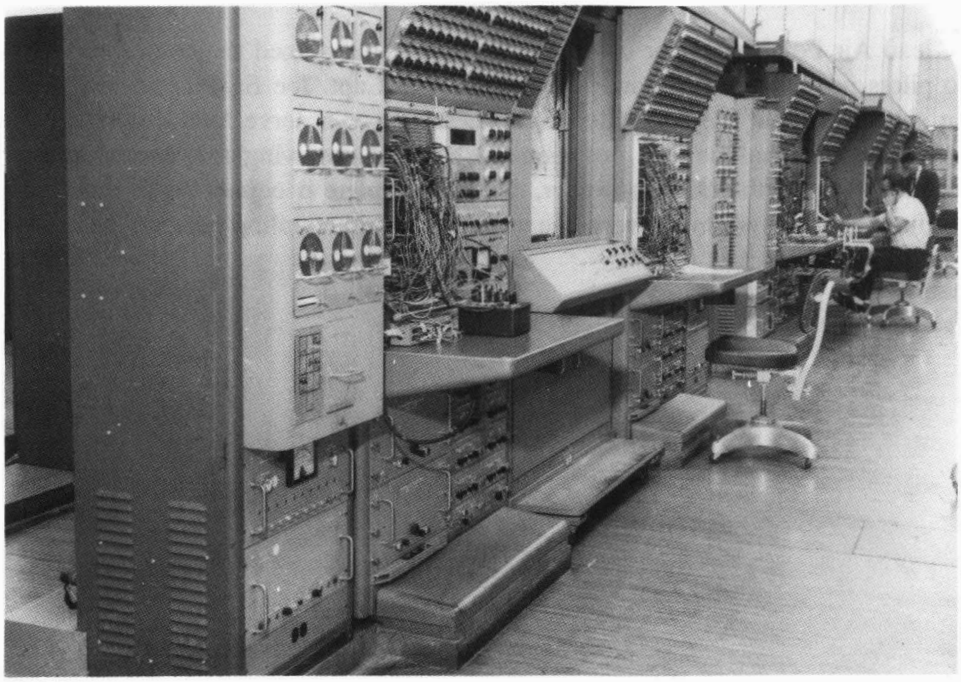

(b) Electronic analog calculating and recording equipment.

Figure 11. The X-15 six-degree-of-freedom simulator.

Development of the Betadot, ($\dot{\beta}$), Control Technique

Shortly after flight planners encountered the adverse control coupling (circa 1959), North American Aviation, Inc., engineer Art Tweedy tried various control techniques on the simulator to tame the control divergences. One of his efforts was to become known as the $\dot{\beta}$ technique. Tweedy, in an effort to make the rate of sideslip zero, nulled the $\dot{\beta}$ equation by pulsing the sidearm controller laterally to oppose the direction of the sideslip needle as it passed through zero. Angle of sideslip, β, was indicated by a crossbar incorporated into the face of the attitude indicator. Positive β was on the right half of the indicator face. When the sideslip needle swings through zero, the rate of change of sideslip, $\dot{\beta}$, is maximum.

The complete $\dot{\beta}$ equation is shown in appendix B. A simplified version containing first-order terms is $\dot{\beta} = -r + \alpha_0 p$. To null $\dot{\beta}$, the side arm controller is pulsed laterally to produce roll at such a rate that $\alpha_0 p = r$, in essence, not allowing sideslip to develop. As the equation indicates, the control technique becomes more effective as α_0 increases, compensating for the increased adverse effect of the second term of the simplified dutch roll equation shown below as α_0 increases (for ventral-on, positive C_{l_β}).

$$C_{n_\beta}^{*} = C_{n_\beta} - \alpha_0 \frac{I_z}{I_x} C_{l_\beta}$$

Tweedy became extremely adept at controlling the X-15 simulations during steep, high-angle-of-attack dampers-off entries. The X-15 pilots watching Tweedy's performances were impressed and attempted to learn the technique. Some were successful, and some were not; however, "flying" a fixed base simulator and flying an airplane are not always equivalent. This control technique was comparable to a sensitive juggler's trick and, like juggling, an appreciable distraction could result in failure. Consequently, the F-100C variable stability airplane was programmed to simulate the X-15 characteristics to evaluate the $\dot{\beta}$ control technique in flight. Figure 10 shows a typical time history of this control technique.

Robert Hoey, lead Air Force engineer on the X-15 project, introduced the control technique to some of the X-15 pilots. Two pilots in particular, Major Robert White and Capt. Joe Engle, became so adept at controlling ground and flight simulators that they considered the method would serve as a backup in case of roll damper failure. Fortunately, the $\dot{\beta}$ technique was not required because removing the ventral solved the dampers-off controllability problem. It is worth noting, however, that the complete $\dot{\beta}$ equation was later used in the yaw channel of the Space Shuttle control system to overcome unstable control coupling (chapter 3).

CHAPTER 3
SIMULTANEOUS COUPLING MODES
SHUTTLE AIRCRAFT

CONTROL COUPLING + DUTCH ROLL COUPLING

Chapter 1 described three X-2 sequential coupling modes. Each was unstable, one mode leading directly to another with disastrous results. Chapter 2 described two X-15 simultaneous coupling modes with dutch roll contributing to dynamically unstable control coupling. During the Space Shuttle entry, two coupling modes occur simultaneously. One mode is stabilizing (dutch roll), the other is destabilizing (control coupling). In chapter 2, the X-15 coupling parameters were a stable C_{n_β} and an unstable C_{l_β}. In the discussion below, the Space Shuttle coupling parameters are reversed, unstable C_{n_β} and stable C_{l_β}. A three-view drawing and a photograph of the Space Shuttle are shown in figure 12. Mass properties pertinent to coupling dynamics are shown in appendix A.

Aircraft are normally flight tested with incremental advances in speed, load factor, etc., that are consistent with safety of flight. These tests either demonstrate airworthiness or indicate modifications required for continued testing. The Space Shuttle did not have the luxury of incremental flight testing except in the low subsonic regime during the air-launched test flights from the Boeing 747 carrier aircraft. The Space Shuttle was forced to "sink or swim" as it encountered an unprecedented span of aerodynamic variables during its first entry flight. The predicted

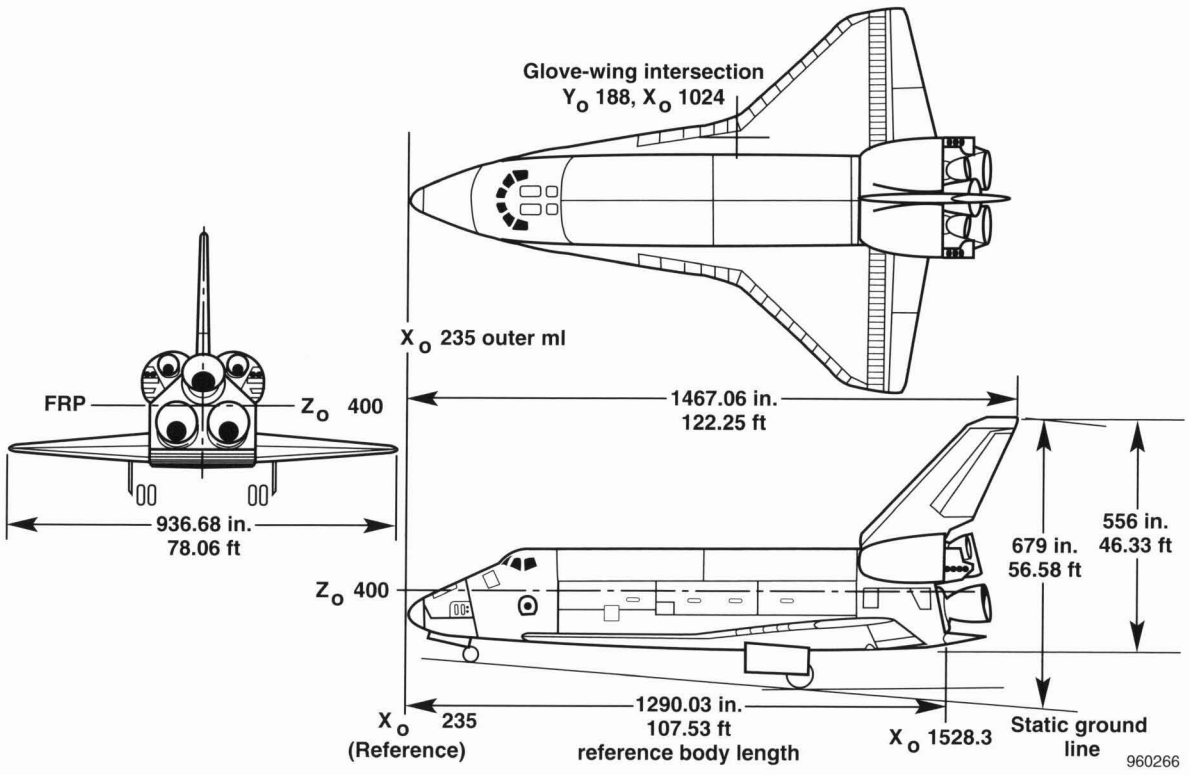

(a) Three view drawing.

Figure 12. Three-view drawing and photograph of the Space Shuttle.

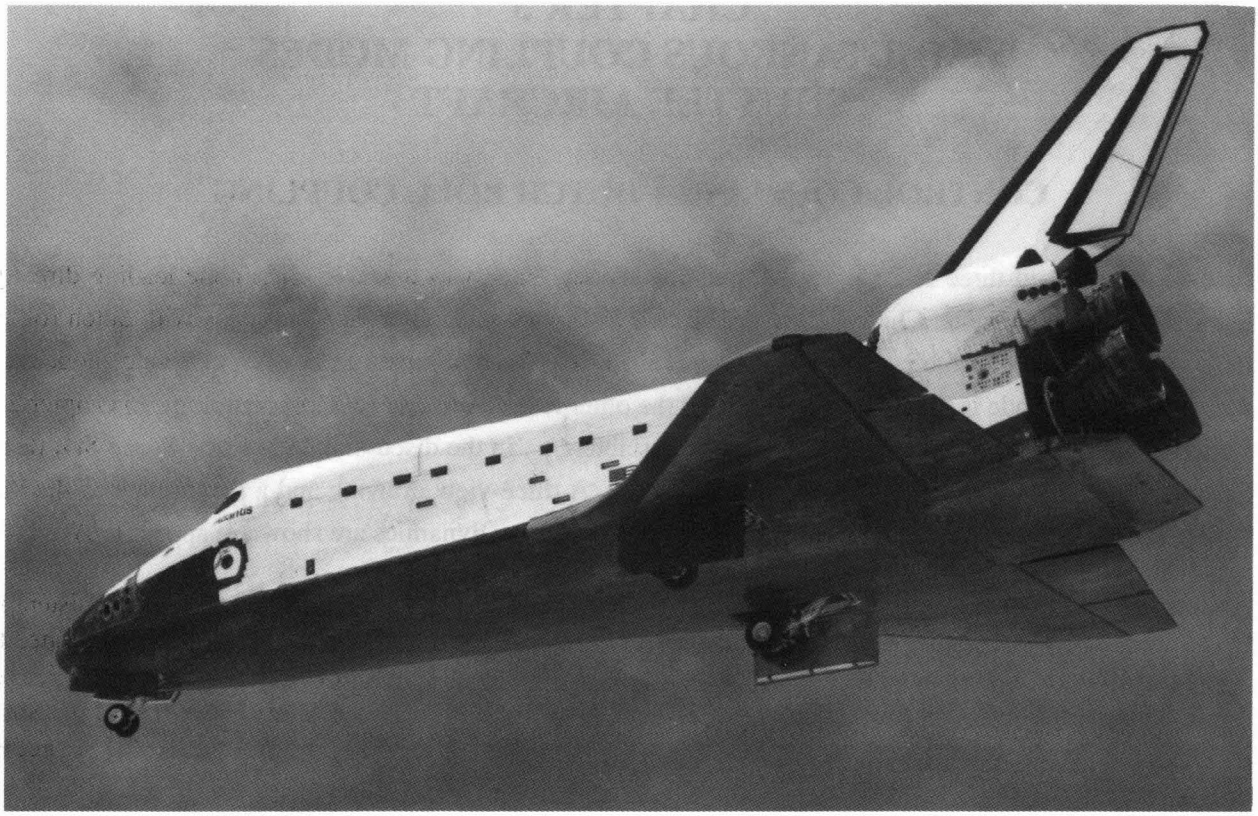

EC 89-0100-001

(b) Photograph.

Figure 12. Concluded.

behavior of the aircraft was predicated entirely on previous ground tests and analyses. The following analysis of the Space Shuttle coupling modes was based on such data and was made before STS 1, the first entry flight.[§]

The entry phase of the Space Shuttle has several problematic characteristics which contribute to coupling dynamics. This chapter describes these problems and their resolution. During the hypersonic and supersonic phases of the entry, the Space Shuttle is plagued by unstable or nonexistent stability and control parameters. The ingenious, and sometimes serendipitous, manner in which these problems were solved is also described in this chapter. Several figures in the following discussion show wind-tunnel values of Shuttle primary stability and control derivatives as a function of Mach number, angle of attack, and elevon position.[10] The solid circles located on these figures indicate derivative values for the angle-of-attack schedule of the entry phase of flight (fig. 13).

DUTCH ROLL COUPLING MODE

This section describes the dutch roll coupling mode of the Space Shuttle as it is influenced by longitudinal stability, directional control and stability, and lateral stability.

[§]Day, Richard E., "Space Shuttle Orbiter Flight Control and Guidance," unpublished presentation given at Flight Control and Guidance Seminar, Stanford University, Palo Alto, California, October 26, 1977.

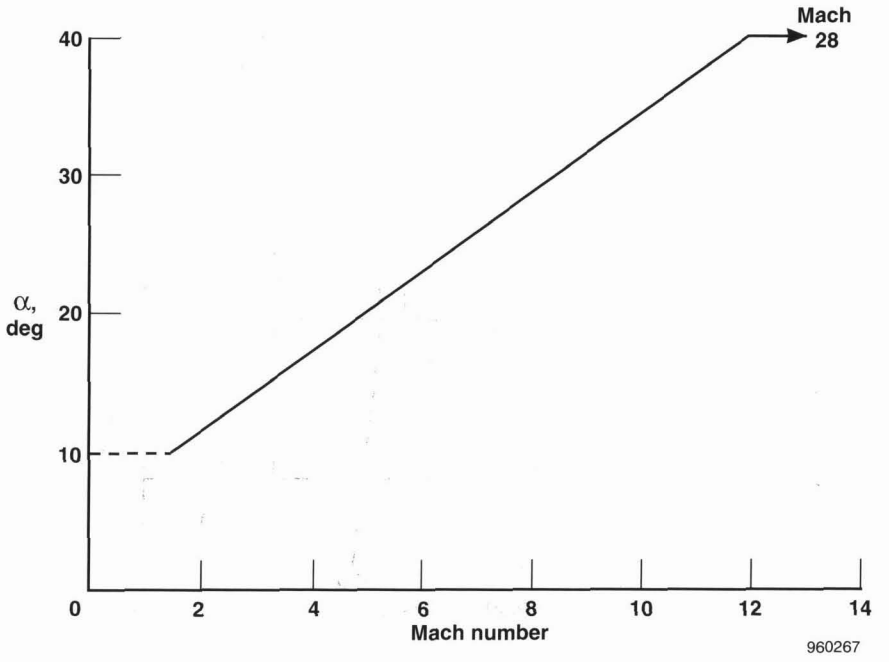

Figure 13. Linear transition of angle of attack with Mach number for proposed first orbital flight of Space Shuttle.

Longitudinal Stability

The initial hypersonic portion of the Shuttle entry regime is designed, primarily from heating considerations, to be flown at extreme angles of attack. In addition to thermal protection, the high angles of attack serendipitously provide longitudinal stability and lateral–directional dutch roll stability. Figure 13 depicts the entry angle of attack as a function of Mach number. A constant angle of attack of 40° is flown to Mach 12 where a linear transition is flown to 10° angle of attack at approximately Mach 1.5.

Figure 14 shows pitching moment as a function of angle of attack at various Mach numbers. The solid circle symbols connected with dashed lines indicate the degree of pitching moment at various Mach numbers during entry. With proper entry profile design, avoiding the longitudinal instability problems through entry to landing is possible. Unfortunately, providing lateral–directional stability and control is not as simple.

Directional Control

The hypersonic high angle of attack that was so beneficial in the longitudinal mode of the Shuttle unfortunately blankets the tail and reduces directional control effectiveness to the vanishing point (fig. 15). Here again, the solid symbols indicate the angle-of-attack schedule with Mach number. At the angles of attack flown, the rudder does not start to become effective until speed is reduced to Mach 8. As speed and angle of attack are further reduced, the rudder is activated at Mach 5 at a moderate value of effectiveness to assist in the *lateral* control and yaw damping. The yaw RCS is active down to approximately Mach 1 in providing or assisting lateral–directional control.

It is rather unfortunate that such a prime controller as the rudder is ineffective in the high-speed regime because, as will be discussed later, the directional stability and yaw due to aileron are both adverse, producing adverse control coupling.

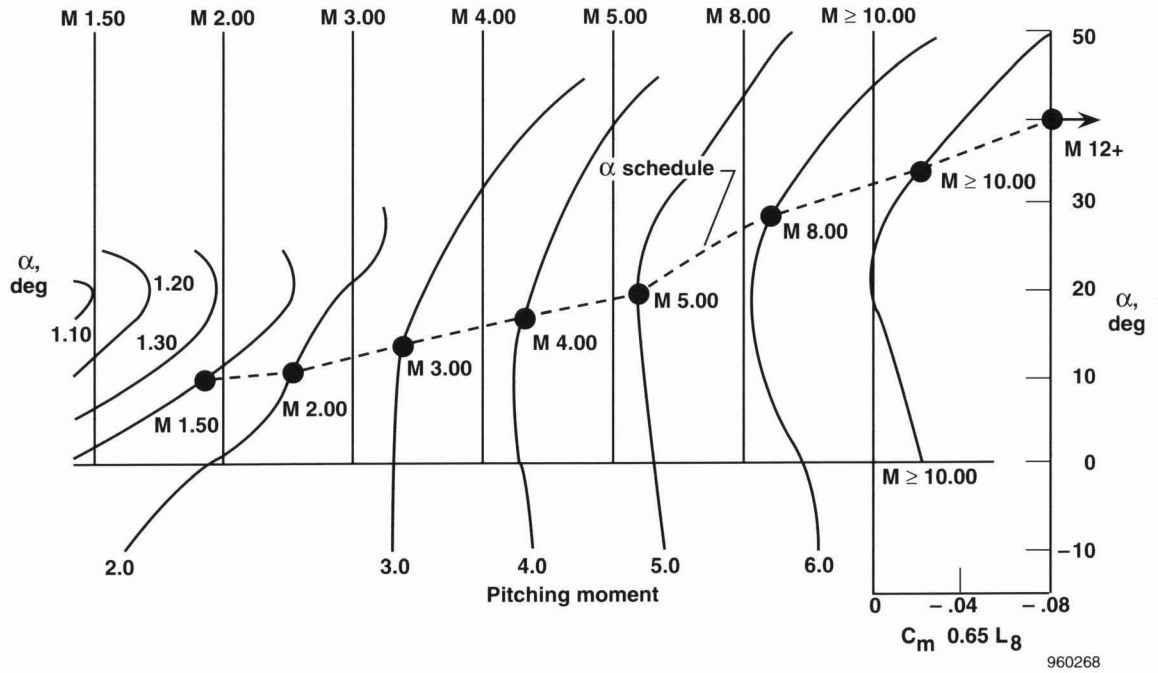

Figure 14. Pitching moment coefficient as a function of angle of attack at various Mach numbers for the Space Shuttle.

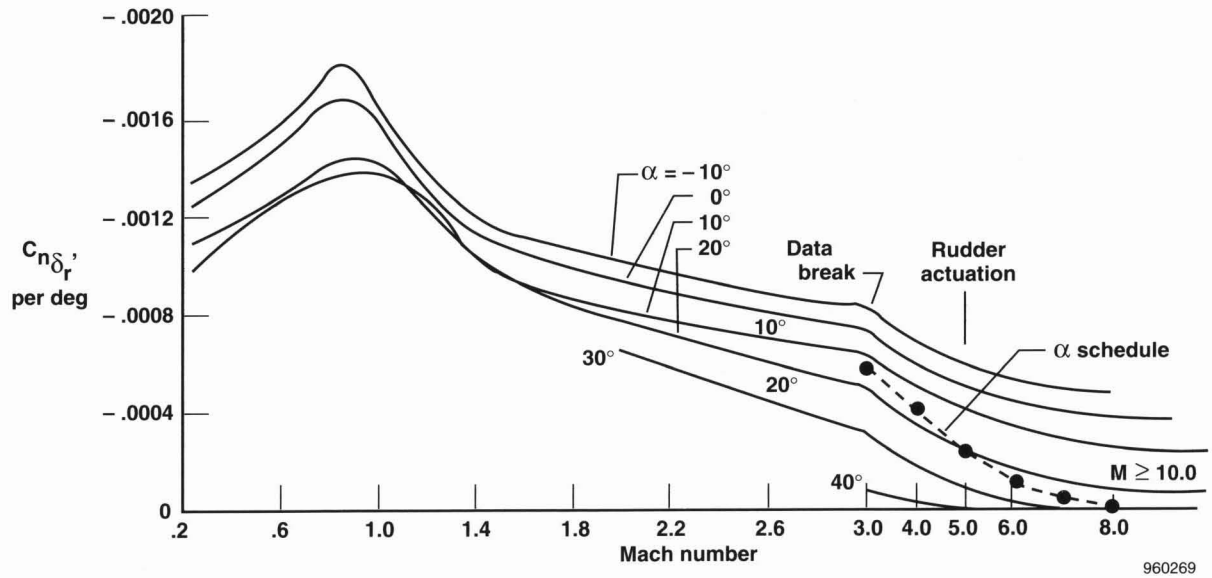

Figure 15. Yawing moment due to rudder deflection for the Space Shuttle.

Directional Stability

Figure 16 shows the Shuttle directional stability as a function of angle of attack at various Mach numbers. The solid symbols indicate C_{n_β} for the angle-of-attack entry schedule. For normal aircraft, the designer attempts to provide a value of C_{n_β} of approximately 0.001 or 0.002, depending on reference geometry and moment of inertia.

In figures 16 and 17, this level of *instability* ($C_{n_\beta} < -0.001$) exists over the major portion of the entire flight regime. With little or no rudder power and directional instability, the control possibilities look somewhat grim.

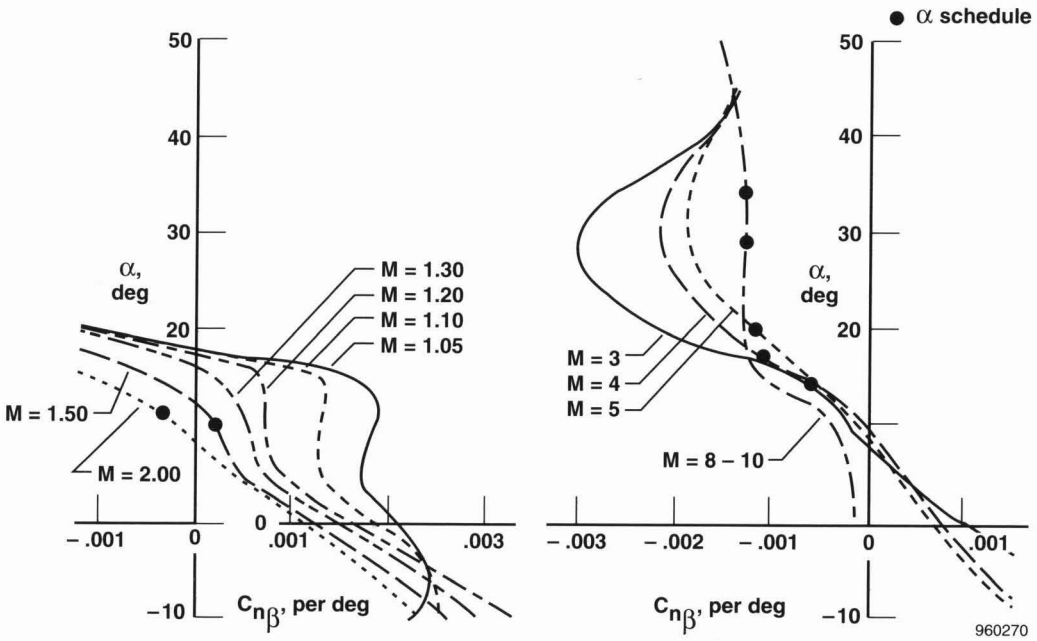

Figure 16. Mach carpet of directional stability derivative versus angle of attack for Space Shuttle.

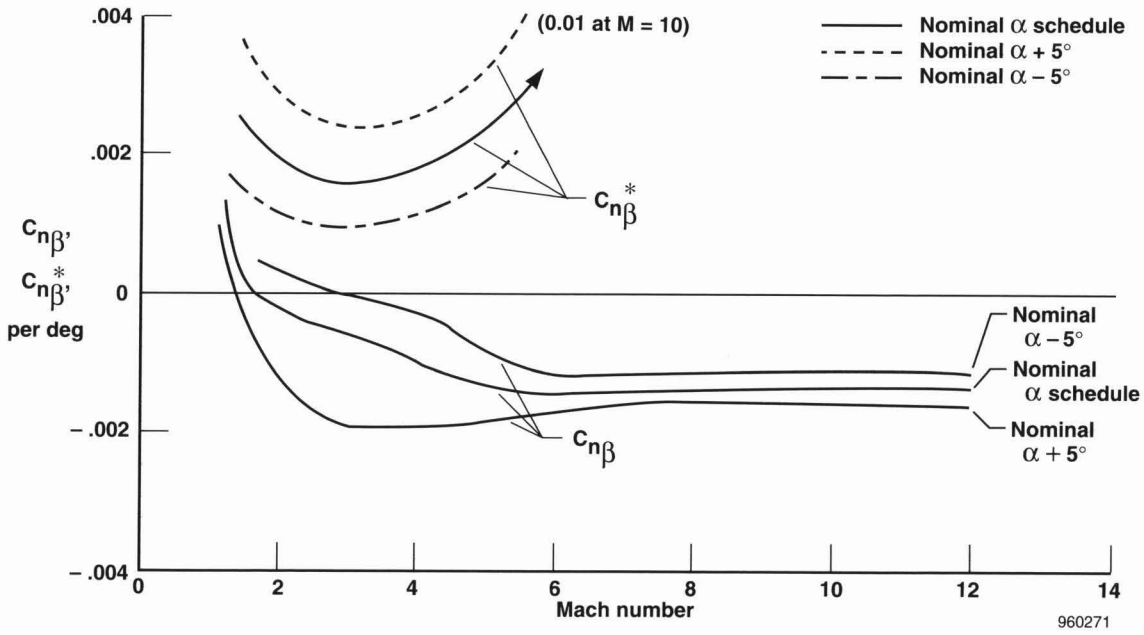

Figure 17. Body axis and dutch roll stability coefficients vs. Mach number at nominal and ±5° entry schedule of Space Shuttle.

Lateral Stability

The Shuttle lateral stability, however, is quite well behaved as might be expected from a highly swept delta-wing. The values of C_{l_β} are always negative (positive dihedral effect) and of relatively high value (fig. 18). Examination of the combined effects of lateral and directional stability in the dutch roll coupling mode reveals that the prospects for achieving stability appear somewhat improved.

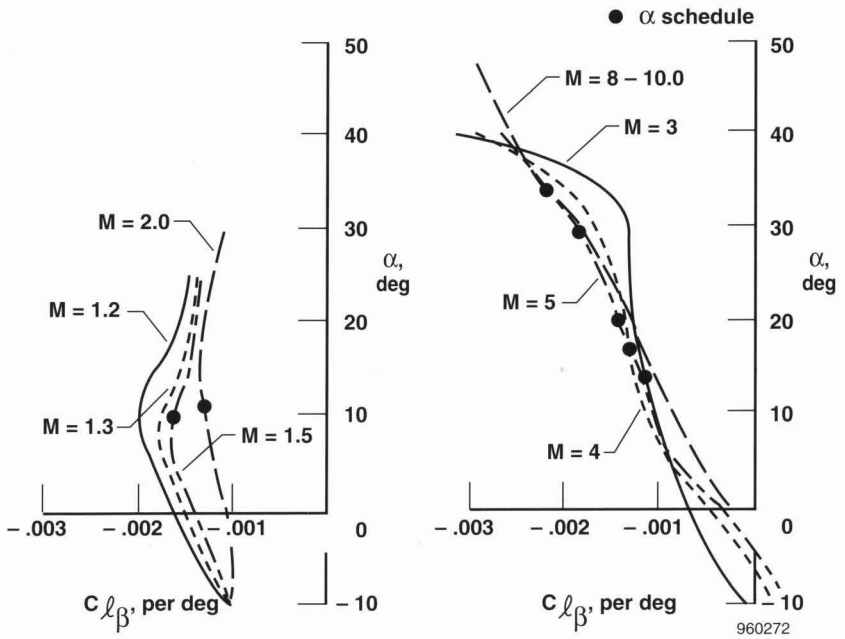

Figure 18. Mach carpet of rolling moment coefficient vs. angle of attack for Space Shuttle.

Dutch Roll Stability

The X-15 dutch roll mode was discussed in chapter 2. Mathematical derivations and the historical development of this parameter are treated in appendix D. The dutch roll equation, $C_{n_\beta}{}^*$, is shown at the top of table 1. To indicate how powerful are the inertia ratio I_z/I_x, trim angle of attack, and C_{l_β} in overcoming deficient C_{n_β}, values of $C_{n_\beta}{}^*$, C_{n_β}, and C_{l_β} are shown in table 1 for trim angles of attack at four Mach numbers. This information is shown in figure 17 with C_{n_β} and $C_{n_\beta}{}^*$ plotted as functions of Mach number at scheduled and ±5° angle of attack which indicates that large values of directional *instability* exist during most of the profile but even larger values of dutch roll *positive* stability are always present.

The same information is presented in yet another form in figure 19, showing stability as a function of angle of attack at Mach 10. Values of $C_{n_\beta}{}^*$ for the basic C_{n_β} and C_{l_β} are shown. The $C_{n_\beta}{}^*$ is also computed for two values of C_{n_β} based on uncertainties ΔC_{n_β} in the predicted data. These figures show the powerful effect of increased angle of attack on stabilizing dutch roll even when large and improbable uncertainties exist. Similar trends in the data exist down to Mach 1.5.

Table 1. Shuttle lateral–directional (dutch roll) stability. (For positive stability, dutch roll stability, $C_{n_\beta}^*$, must be > 0.)

$$C_{n_\beta}^* = C_{n_\beta} \cos\alpha_0 - I_z/I_x C_{l_\beta} \sin\alpha_0$$

Shuttle $I_z/I_x = 7.7$

	Derivatives, per degree			
Mach number	1.5	3.0	5.0	10.0
α_0	10.0	14.0	20.0	34.0
C_{n_β}	0.00025	–0.0006	–0.00125	–0.0013
C_{l_β}	–0.0016	–0.00115	–0.0014	–0.0025
$C_{n_\beta}^*$	0.0024	0.0016	0.0025	0.0097

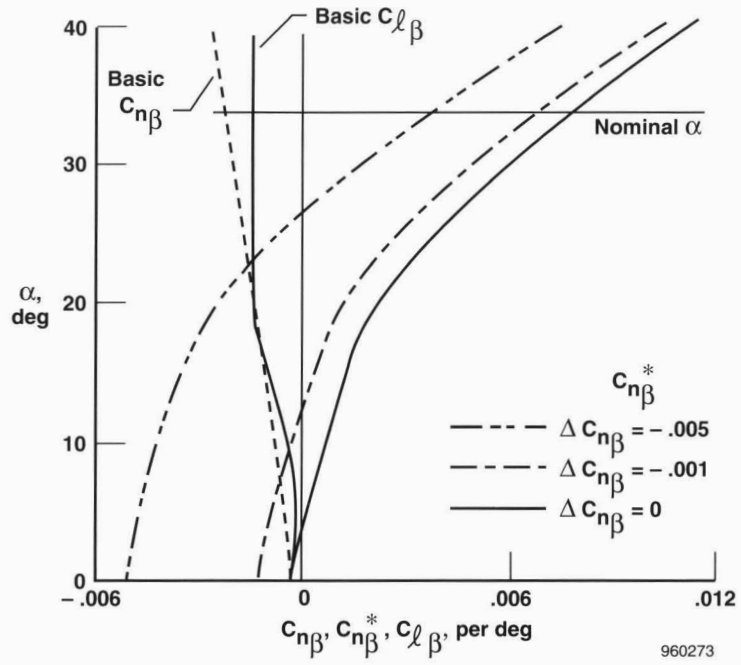

Figure 19. Space Shuttle directional stability, Mach 10.

It must be remembered that the dutch roll stability shown here is for stick-fixed oscillations. Any attempt to damp roll velocity has the same effect as reducing the inertia ratio or the effective dihedral and, consequently, the stability. However, as shall be discussed later, the level of stability is sufficiently high that a portion of it has been sacrificed to permit damping.

The X-15 also trimmed at high angles of attack for entry. The X-15, however, was adversely affected by $C_{n_\beta}^*$. The X-15 dutch roll stability is discussed in chapter 2.

CONTROL COUPLING MODE

Lateral–Directional Control

Figures 20 and 21 indicate the level of Shuttle aileron effectiveness in roll and yaw as a function of elevon position and angle of attack at various Mach numbers. The solid symbols indicate the derivative value at trim elevon position for the entry angle-of-attack schedule shown in figure 13.

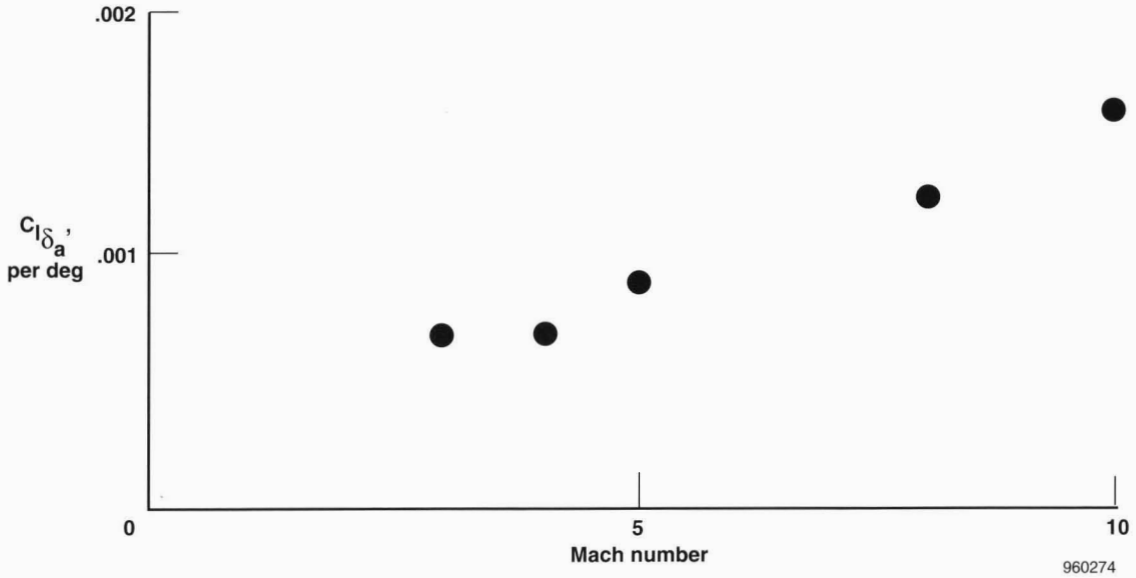

Figure 20. Roll due to aileron coefficient, $C_{l_{\delta_a}}$, for angle-of-attack entry schedule of Space Shuttle.

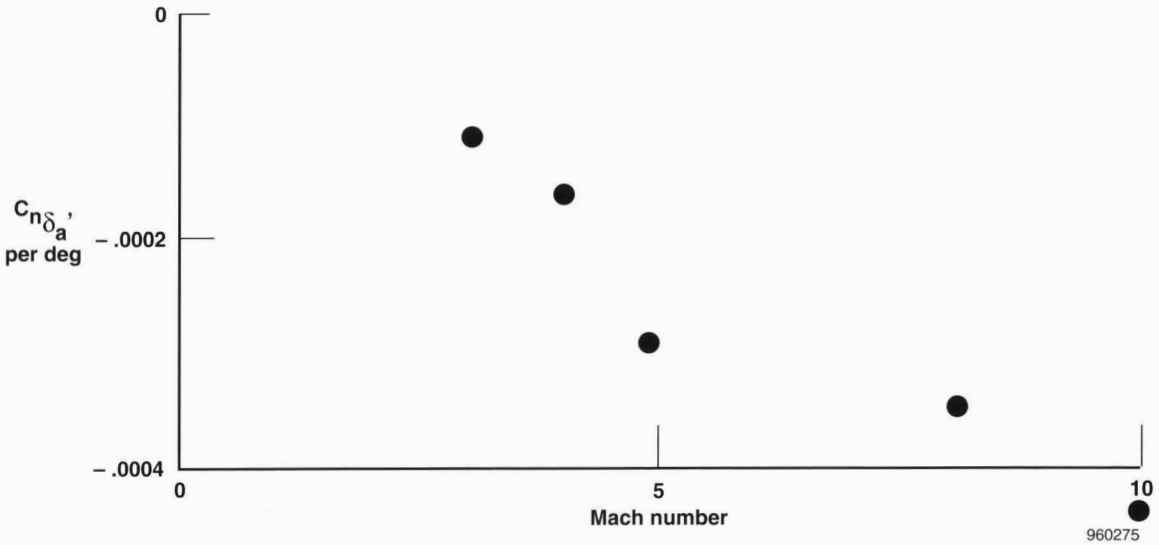

Figure 21. Yaw due to aileron coefficient $C_{n_{\delta_a}}$, for angle-of-attack entry schedule of Space Shuttle.

Figure 20 shows that roll due to aileron, $C_{l_{\delta_a}}$, is always positive and generally increases with increasing angle of attack and elevon position. This effect is normal and desirable; however in addition to rolling the airplane, aileron deflection also produces yaw and, as Murphy would have it, yaw in the wrong direction. This adverse yaw due to aileron is the most troublesome of all derivatives including negative directional stability and nonexistent rudder effectiveness. Figure 21 shows that yaw due to aileron, $C_{n_{\delta_a}}$, is negative (adverse) during entry down to approximately Mach 2 (Mach 2 not shown).

An explanation of what happens during a Space Shuttle nonaugmented maneuver is quite tedious but not difficult to follow. Note the following explanation of the Space Shuttle control coupling is similar to that of the X-2 described in chapter 1, but it differs quantitatively because the signs of various derivatives are not the same. To initiate right roll, the control stick is deflected to the right and should produce right roll. However, the adverse yaw due to aileron yaws the airplane to the left (positive sideslip). Because directional stability, C_{n_β}, is negative (fig. 16), no restoring moment exists, and sideslip continues to diverge. Remembering that there is a high level of roll due to sideslip, C_{l_β}, the dihedral effect becomes larger than aileron effectiveness, and the airplane rolls to the left. In other words, the airplane rolls in the direction opposite to that commanded by stick position. One might think that to correct the situation either the pilot could be trained to fly "backwards" (this has been done in simulators but is not recommended for flight) or the controls could be electronically reversed. This was accomplished early in the Shuttle program (called control system XI), and the Orbiter was controllable during simulations. However as can be seen from figure 21, if off-nominal maneuvers occur, $C_{n_{\delta_a}}$ can become positive and produce roll reversal using system XI. Also, the system must switch back to nominal as $C_{n_{\delta_a}}$ becomes positive in the lower speed range. It is difficult to predict just when this change will occur because actual flight derivatives are seldom exactly as predicted. Consequently, system XI was abandoned, and system X was adopted. Refer to the Shuttle Entry Control System (System X) subsection for additional information.

Solving the control parameter (CP) inequality for C_{n_β} quantifies this coupling characteristic in terms of the primary lateral–directional derivatives involved (table 2). The control parameter equation can be derived from the roll, yaw, and sideforce equations of motion as discussed and derived in appendix C. The equation, as shown in table 2, states that to maintain positive control, directional stability must be greater than the right-hand side of the inequality. The derivative values in table 2 are taken from previously discussed figures. As the numbers in table 2 indicate, the control parameter produces adverse control during entry.

The previously discussed dutch roll coupling, $C_{n_\beta}{}^*$, which is always positive cannot be substituted for C_{n_β} in the control parameter equation because the former is a control fixed, dynamic parameter. Because $C_{l_{\delta_a}}$ is always positive and C_{l_β} is always negative, the right-hand side of the inequality always takes the sign opposite that of $C_{n_{\delta_a}}$. As a result, an adverse (negative) $C_{n_{\delta_a}}$ is particularly damaging for low values of C_{n_β} and especially so for negative values.

Table 2. Control parameter $C_{n_\beta} > \frac{C_{n_{\delta_a}} C_{l_\beta}}{C_{l_{\delta_a}}}$, *Space Shuttle.*

	Derivative values, per degree			
Mach number	1.5	3.0	5.0	10.0
α trim	10.0	14.0	20.0	34.0
$C_{l_{\delta_a}}$	0.00150	0.00070	0.00090	0.00140
$C_{n_{\delta_a}}$	0.00035	–0.00010	–0.00030	–0.00045
C_{l_β}	–0.00160	–0.00115	–0.00140	–0.00250
C_{n_β}	0.00025	–0.00060	0.0	–0.00130
Right side of inequality	–0.0007	0.00016	0.00047	0.00080

As shown in appendix C, the control parameter is dependent on the nondimensional, lateral–directional stability and control derivatives and is independent of physical quantities, such as airspeed, altitude, dynamic pressure, mass, inertia, and body dimensions. This indicates that if the control parameter is neutral or negative, the aircraft is untrimmable or uncontrollable without outside influences, such as reaction controls.

The supposedly control-configured Space Shuttle cannot make it on aerodynamic control surfaces alone (table 2). To implement controllability, the system must rely on the reaction control rockets.

Shuttle Entry Control System (System X)

To overcome the difficulties described above, the lateral–directional control system was designed around the "betadot" equation of motion (appendix B). Roll is commanded in the normal manner by deflecting the rotational hand controller (RHC) to the right or left. However instead of going to the ailerons which would produce control reversal, the signal goes to the yaw jets to produce sideslip and roll due to sideslip (C_{l_β}) and exits as roll command to the "early entry" yaw channel.

In the yaw channel, turn coordination ($\frac{g}{V}\sin\phi\cos\theta$) is summed with yaw rate ($-r$) then summed with the product of roll rate and sine of angle of attack ($p\sin\alpha$) to produce the first-order terms of the betadot equation:

$$\dot{\beta} = \frac{g}{V}\sin\phi\cos\theta - r\cos\alpha + p\sin\alpha$$

The variables of the equation are derived from onboard instrumentation. The lateral–directional control system switches from "early entry" (dynamic pressure in excess of 20 lb/ft^2 to Mach 1.5) to "late entry" (Mach 1.5 to subsonic). At which point, nominal control is assumed.

As stated earlier, the Space Shuttle did not have the luxury of incremental flight testing from hypersonic entry to low subsonic speeds. Predicted behavior of the aircraft was based almost entirely on previous ground tests and analyses. In addition, to maintain a sense of conservatism, many simulator studies were made using degraded aerodynamic parameters.[¶]

[¶]Thompson, Milton O., Bruce G. Powers, Richard E. Day, Timothy W. Horton, and Joseph Weil, "An Assessment of the Orbiter Entry Flight Control Characteristics with Degraded Aerodynamics," unpublished working paper, February 1981.

Figure 22 shows the four lateral–directional stability and control derivatives involved in the Space Shuttle coupling incidents.[11] These data were obtained during the first three orbital flights comparing predicted values with flight values. These plots indicate good agreement for the coefficients except for $C_{n_{\delta_a}}$ at some hypersonic speeds. Despite these differences, these ground test data were sufficiently accurate to permit a successful first flight.

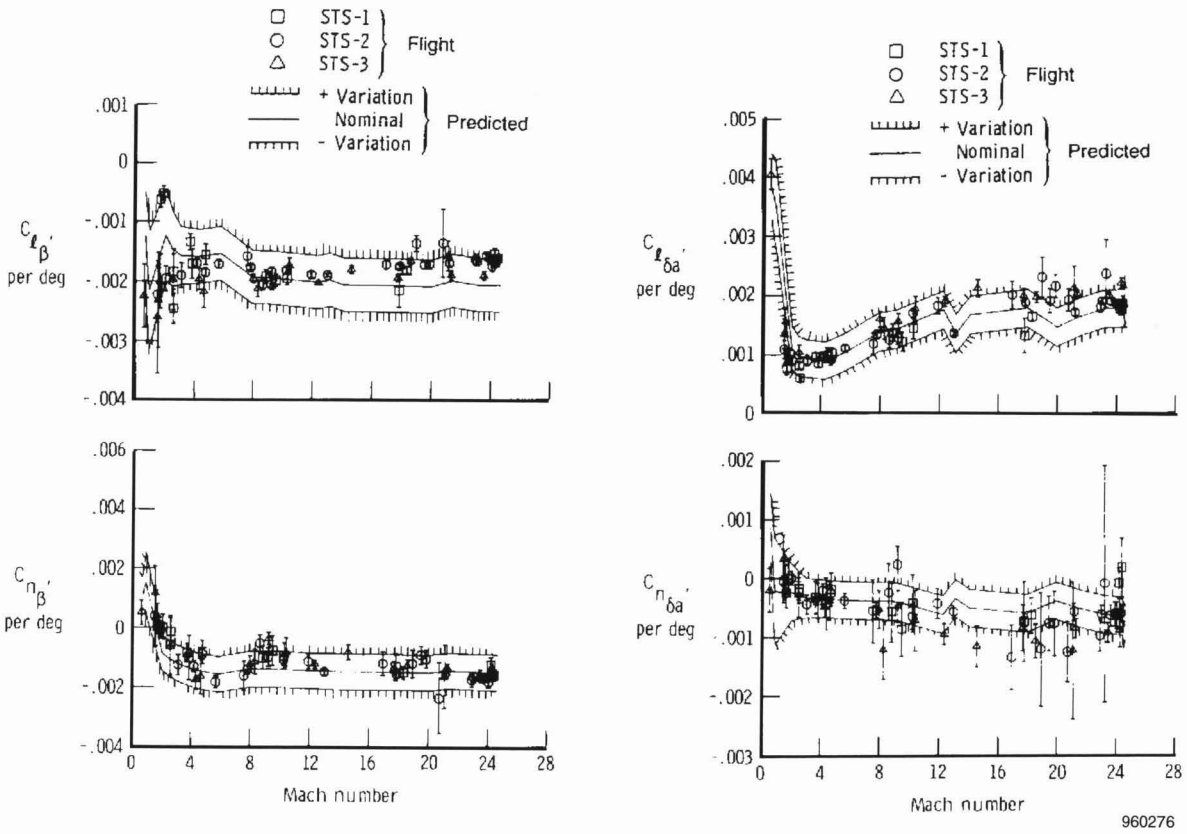

Figure 22. Space Shuttle lateral–directional stability and control derivatives for first three orbital flights.

CHAPTER 4
INERTIAL ROLL COUPLING MODE
X-3, F-100A, YF-102 AIRCRAFT

In 1954, inertial roll coupling made its debut in a series of unexpected, extremely violent motions during rudder-fixed aileron rolls while testing the F-100A and X-3 aircraft. George Welch, NAA chief test pilot, lost his life. In addition, George Smith, NAA pilot, was severely injured after a supersonic bailout during rolling pullouts. Also during that year, NACA pilot Joe Walker experienced violent motions during two rolling maneuvers—one at Mach 0.92 and the other at Mach 1.05 on the same flight. As predicted by Phillips in his 1948 report,[1] these aircraft with heavily loaded fuselages and reduced stability were victims of inertial roll coupling. Appendix E describes the physical and mathematical aspects of inertial roll coupling. The X-2 roll coupling was discussed in chapter 1 as one of three sequential coupling modes.

The F-100A airplane that NACA used for general stability and control testing was, by agreement with the Air Force and NAA, relegated to an intense program of inertial roll coupling testing.[3] After the tests were completed, the NACA High Speed Flight Station published a combined report on the X-3 and F-100A aircraft (NACA RM-H55A13).[12] The Introduction to this February 1955 Research Memorandum states: "The present paper presents the first data with little attempt at analysis since it is felt that data showing this behavior will be of general interest in that other current airplanes might be expected to encounter similar behavior." This Research Memorandum, in a way, was also a tribute to Phillips in that his Technical Note was the only reference citation listed. Phillips' 1948 report and the expedited Research Memorandum, published in February 1955, received wide distribution within the government-industry complex and served as the basis for many studies of inertial roll coupling.

In addition to the X-2 coupling characteristics discussed in chapter 1, the F-100A and X-3 aircraft are prime examples of inertial roll coupling and will provide the bulk of discussion. Table 3 lists the aircraft which encountered violent inertial roll coupling.

Table 3. Chronology of inertial roll coupling incidents.

Date	Aircraft
10/1954	X-3
10/1954	F-100A
--/1955	YF-102
9/1956	X-2

X-3 INERTIAL ROLL COUPLING

The majority of the experimental research airplanes that were designed for supersonic research were rocket powered. The X-3, built by Douglas Aircraft Company, was to be powered by two jet engines that could sustain speeds of Mach 2 and above. Only one aircraft was built. This airplane was delivered to the NACA in 1954 with underpowered interim J34 engines that were unable to achieve supersonic speed in level flight. Speeds beyond Mach 1 could only be attained in power dives. The maximum speed attained by the X-3 was Mach 1.21.[13] More powerful jets did not materialize before the airplane was retired in May 1956.

Using thrust provided by two XLR-11 (Reaction Motors, Inc.) rocket engines (eight chambers) and initial conditions for an air launch, the author calculated that the X-3 could attain Mach 4.2. The Research Airplane Projects Panel (RAPP) did not consider the effort worthwhile in view of the rapidly developing F-104 that would have Mach 2 capabilities and an imminent contract award for the X-15 (June 1956). These calculations, using the

archaic slide rule for graphical construction and a planimeter for integration, required many hours for solution. Today's personal computers can calculate the same problem in a matter of seconds with a greater degree of accuracy. This proposed modification was one of three for extending the performance capabilities of the X-series aircraft into the high supersonic and hypersonic speed regime. The other aircraft were the X-2 (chapter 1) and the X-1E.[3]

A three-view drawing of the X-3 is shown in figure 23(a); a photograph is shown in figure 23(b). For purposes of comparing the coupling properties of the X-3 with other coupling prone aircraft, various mass properties and inertia ratios are listed in appendix A.

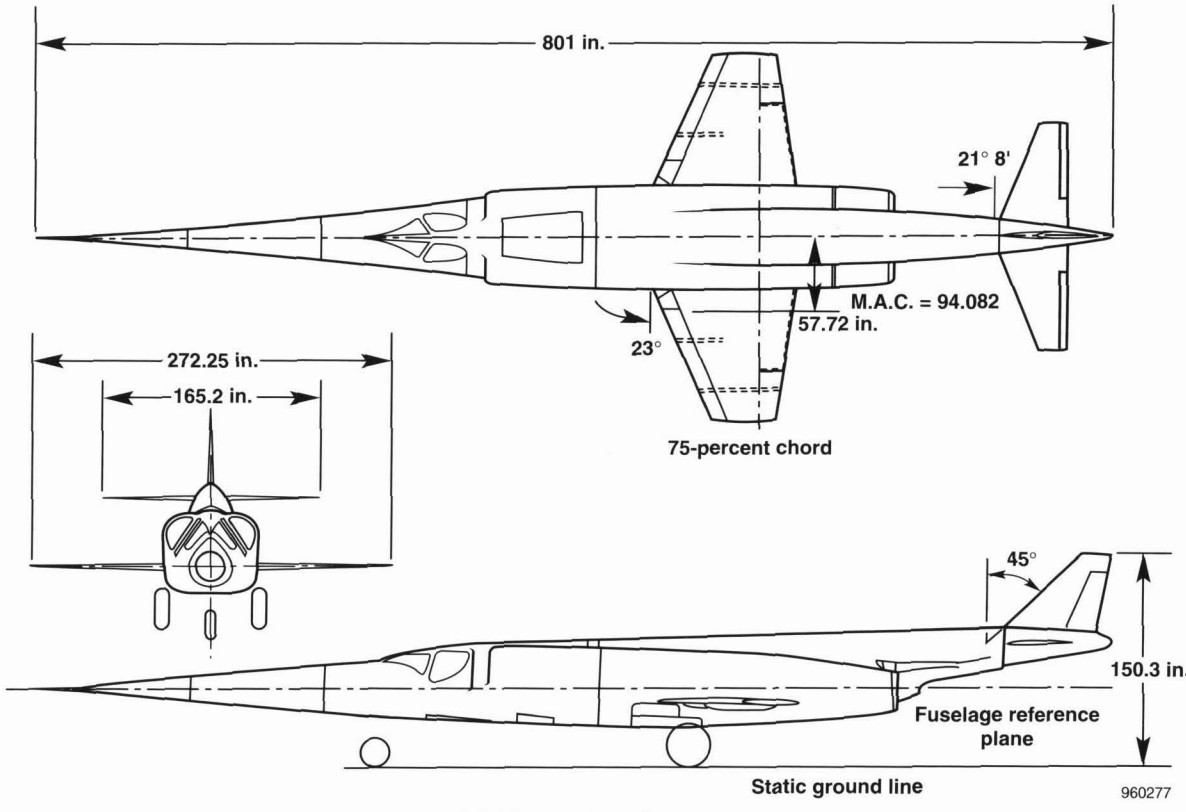

(a) Three-view drawing.

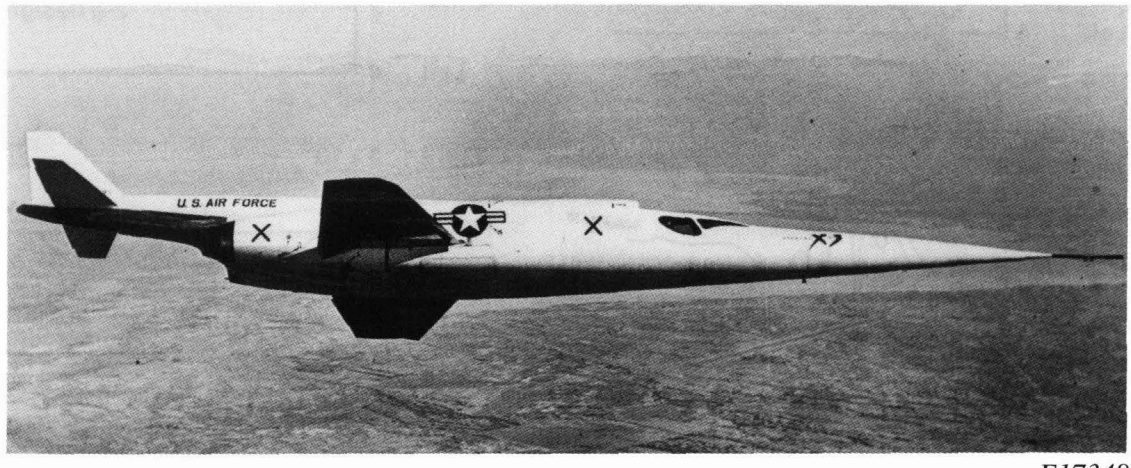

E17348

(b) Photograph.

Figure 23. Three-view drawing and photograph of the Douglas X-3 research airplane.

X-3 FLIGHT TEST PROGRAM

The NACA X-3 flight test program began in August 1954. During the buildup program, stability, control, and loads data were obtained extending to Mach 1.21.[13] The extent of the roll coupling study was extremely short but very productive in terms of valuable data. During the tenth NACA flight, Walker performed two rudder-fixed abrupt aileron rolls. The first roll, performed at Mach 0.92 at an altitude of 30,000 ft, resulted in large excursions in angles of attack and sideslip. Although the motions were quite disturbing, the resulting accelerations were not excessive; consequently, Walker proceeded to the next test point, dove to Mach 1.05, leveled off, and entered into another abrupt aileron roll. The resulting motions were similarly large, but with the increased dynamic pressure and higher values for force derivatives, excessive accelerations and loads were encountered.[12,14]

Stability, Control, and Loads

The time history of stability and control parameters of figure 24 shows sideslip beginning to diverge at time ~ 1 sec as the aircraft reached its critical roll velocity (calculated to be 2.5 rad/sec).[14] When sideslip reached 20°, at time 4 sec, the airplane pitched down to an angle of attack of –13°. Walker immediately pulled back-stick, inadvertently overshooting to a positive 19° angle of attack. When controls were neutralized, the motion subsided. Figure 24 also indicates the violent accelerations and loads imposed during the short time span of the maneuver.[14] Normal acceleration, a_n, peaked at ±7 g. Transverse acceleration, a_t, peaked at –2 g. Design acceleration loads and 50 percent of vertical tail shear load were demonstrated in a span of approximately 1 sec.

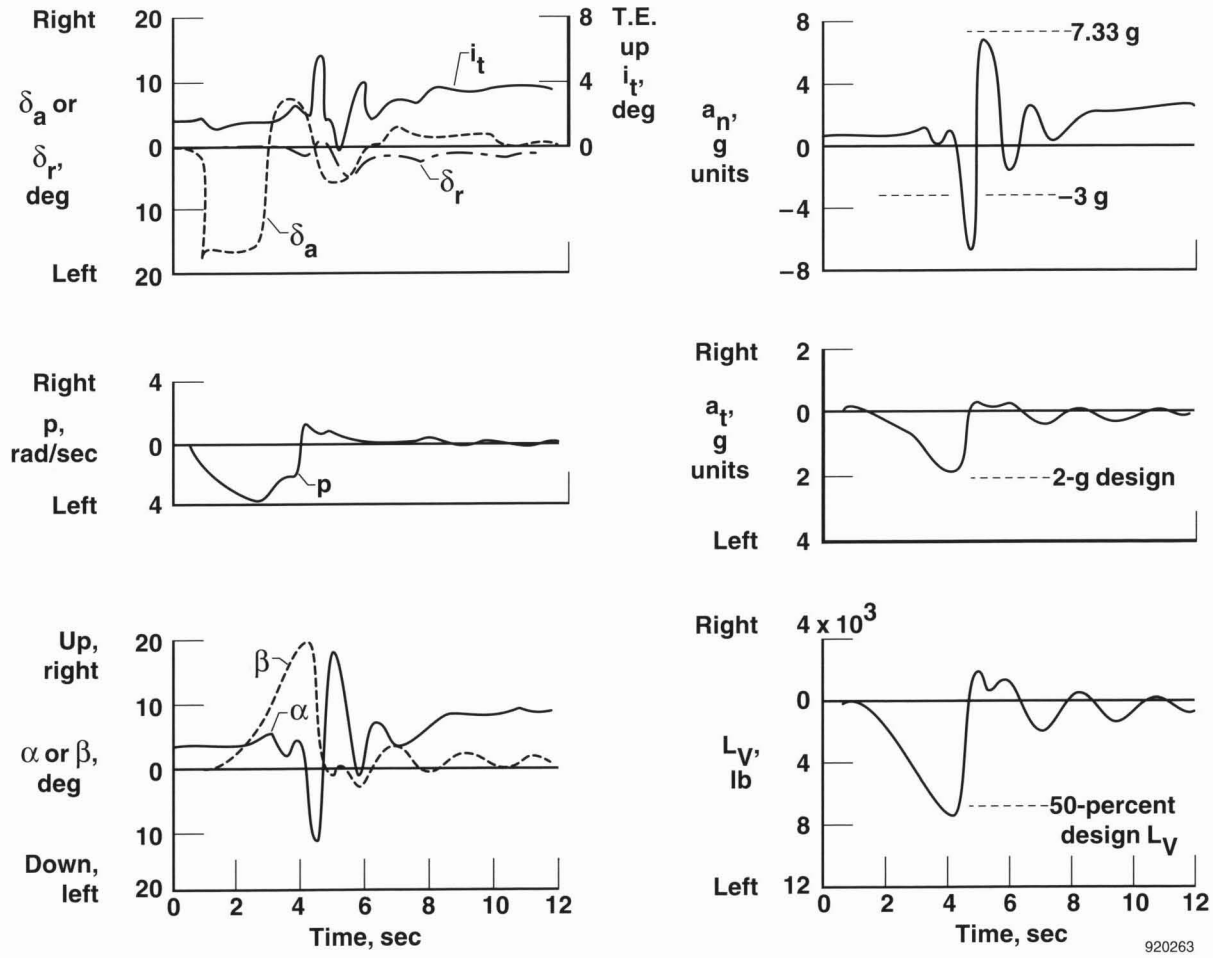

Figure 24. Time history of X-3 abrupt aileron roll, Mach 1.05 and pressure altitude 30,000 ft.

F-100A INERTIAL ROLL COUPLING

The F-100A, one of the early Century series fighter aircraft, was configured with a single turbojet engine and a low swept wing and tail. The F-100A, like the X-3, had a highly loaded, high-fineness-ratio fuselage. Unlike the X-3, the F-100A had sufficient thrust to attain supersonic speed in level flight and Mach 1.48 in shallow dives.[15] In 1954, the HSFS received an early production model of the F-100A for general stability and control evaluation. At about this time, the X-3 and F-100A aircraft in the field were experiencing violent motions about all three axes during rudder-fixed aileron rolls. Phillips theoretical report[1] that was previously thought to have been only an intellectual exercise, now loomed large as a key to the probable causes of, and solutions to, the current problem — inertial roll coupling. Walt Williams, director of the HSFS, dispatched engineers Hubert Drake and Joe Weil to Langley Research Center to confer with Phillips and observe five-degree-of-freedom analog computer runs which confirmed that marginal directional stability was, indeed, the culprit catalyzing the violent motions during rolling maneuvers.

Because low directional stability was demonstrated to be the villain, a program for fabricating a larger vertical tail was started immediately. Under pressure from the NACA and the Air Force, NAA cut its delivery schedule from 90 days to just 9 days.[3] Figure 25(a) shows a three-view drawing of the airplane with the original tail. Figure 25(b) is a photograph of the airplane with the original vertical tail. Mass properties and inertia ratios pertinent to coupling modes are listed in appendix A.

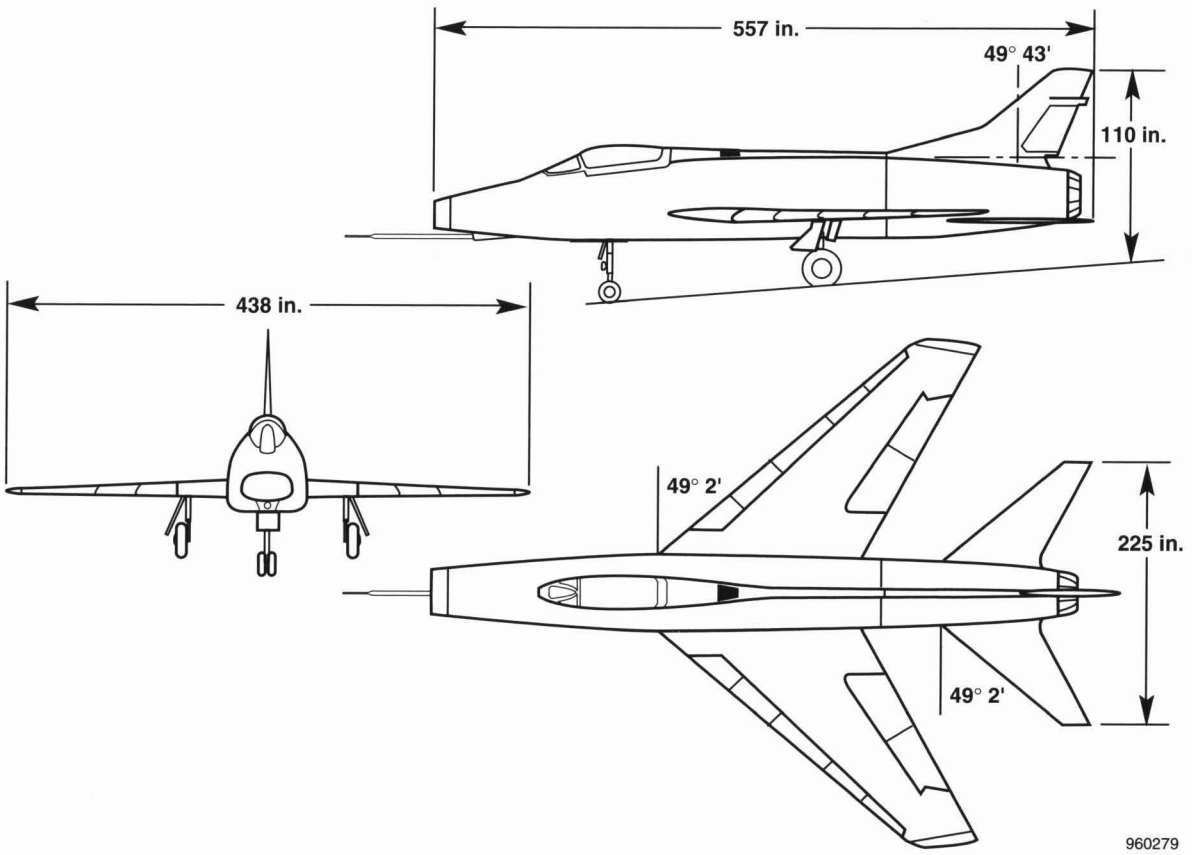

(a) Three-view drawing.

Figure 25. Three-view drawing and photograph of the F-100A (original vertical tail).

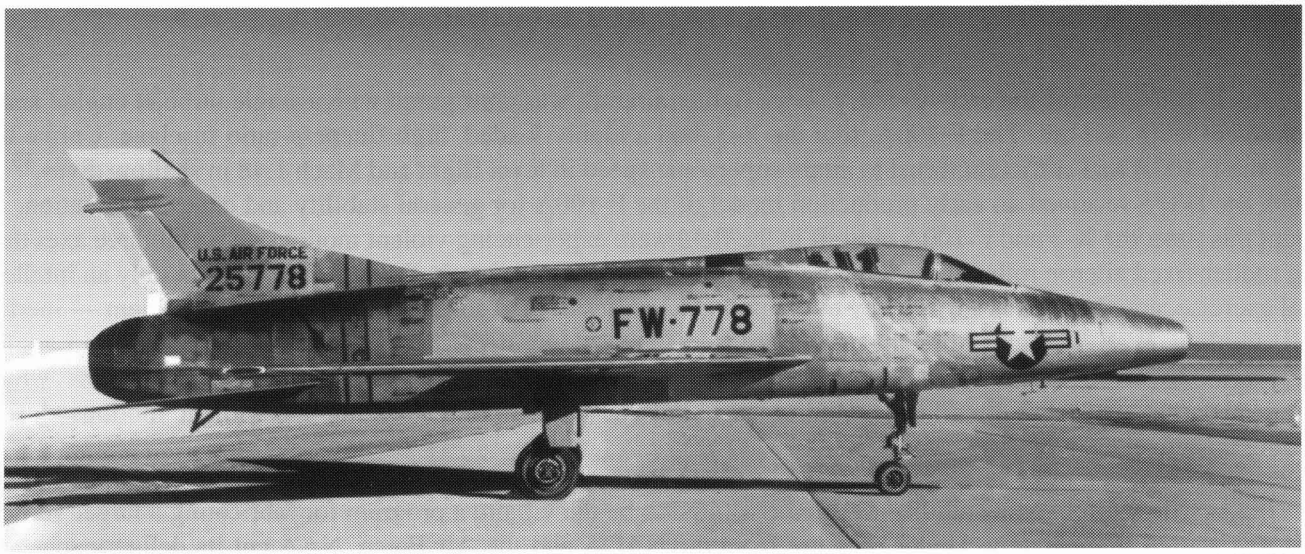

EC 87522

(b) Photograph.

Figure 25. Concluded.

F-100A FLIGHT TEST PROGRAM

In a period of three months from October through December 1954, HSFS test pilot Scott Crossfield demonstrated the coupling boundaries of the F-100A configured with the original tail and with two other tails of increased area and aspect ratio. One particular coupling incident which occurred at Mach 0.7 at an altitude of 32,000 ft (tail A) generated six Research Memorandums[12–17] within the HSFS alone, including the initial motivating report, mentioned at the beginning of this chapter. The following discussion is taken from these six reports.

Stability and Control

Five months after publication of reference 14, a more detailed analysis of the coupled motions of the original incident was published in reference 16. A time history of the abrupt aileron roll taken from this reference is presented in figure 26(a). Almost immediately after aileron input, sideslip and angle of attack began to diverge negatively. Between time 3 and 4 sec, the rates of divergence increased rapidly, and the airplane became uncontrollable. When the controls were returned to neutral, the motions subsided. During the coupled divergences, an angle of sideslip of –26° was attained, and angle of attack went off scale at –16°. Roll velocity, p, could not be correlated with resonant frequencies because of instrumentation failure.

Directional Stability

Because the pitch and yaw natural frequencies of the airplane determine the resonant roll rate for inertial roll coupling, it was necessary to obtain flight values of body axis directional stability, C_{n_β}, for all three tail configurations in order to calculate and predict roll coupling behavior. The values of C_{n_β} used during the F-100A flight test program were obtained from the dutch roll equation developed in reference 15 and summarized in appendix D.

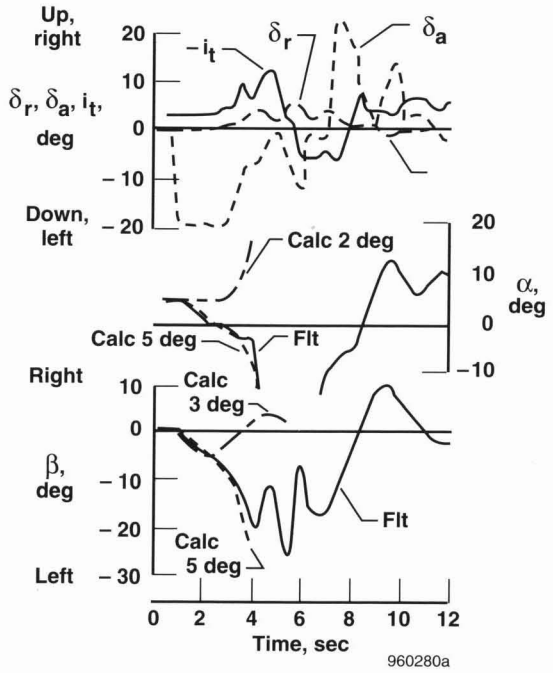

(a) Stability and control parameters during coupled motions.

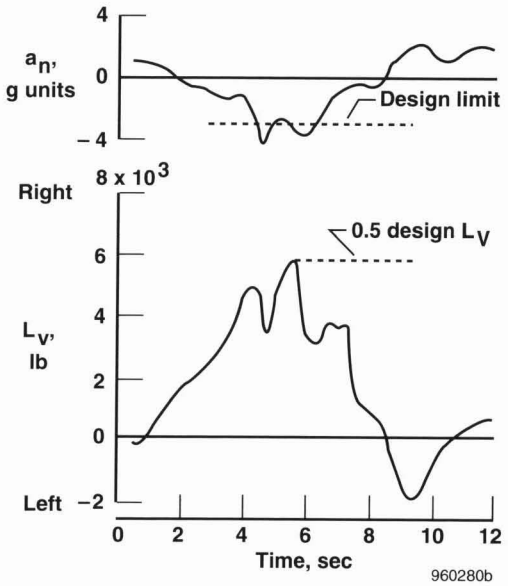

(b) Load and acceleration parameters during coupled motions.

Figure 26. Time history of F-100A abrupt aileron roll, Mach 0.7 and pressure altitude 32,000 ft.

A sketch of the three vertical tails is shown in figure 27. Tail B was enlarged by 11.3 percent and tail C was enlarged by 27.5 percent over the original tail A. Tail C roughly doubled the directional stability of tail A through the Mach number range as shown in the lower part of figure 27. The effect of increasing the vertical tail size as revealed by left aileron rolls is shown in figure 28. Shown are the maximum change in angles of attack and sideslip at the first peak as a function of maximum roll rate. The violent maneuver with tail A (fig. 28) is indicated on the plot by a circular symbol. Dashed lines show the results obtained from the five-degree-of-freedom calculations. Figure 27 indicates a successive degree of improvement with increasing tail size. The airplane, modified with the larger tail, returned to field service with little or no further inertia roll coupling incidents.

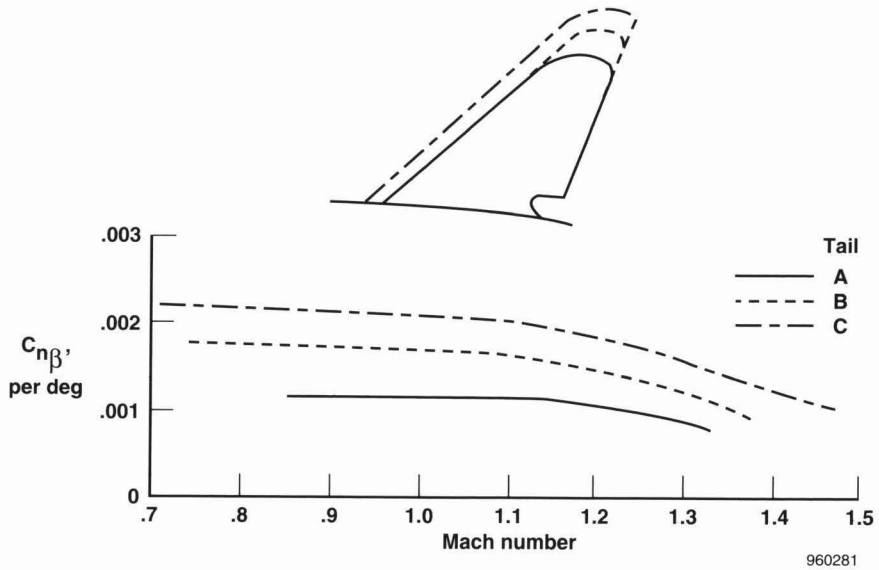

Figure 27. F-100, effect of tail size on flight-derived directional stability vs. Mach number.

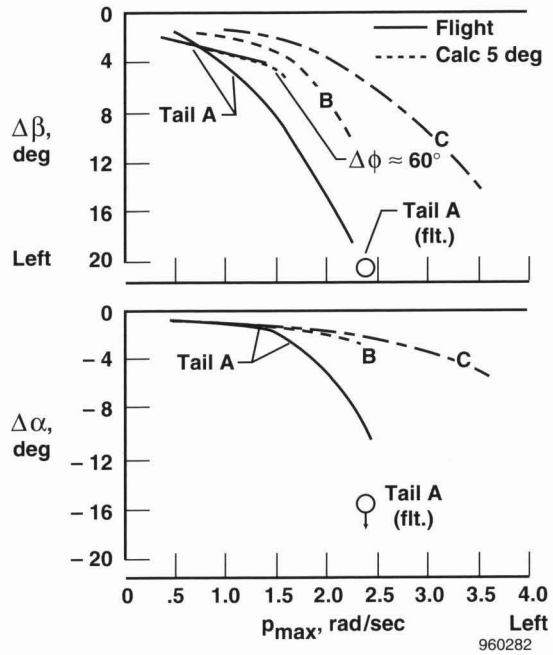

Figure 28. F-100, effect of tail size on left aileron rolls, Mach 0.7 and pressure altitude 31,000 ft.

Loads

At time 4.5 sec (fig. 26(b)), a normal acceleration, a_n, of –4.4 g exceeded the design limit by 50 percent, and although the sideslip angle reached –26°, lateral acceleration, a_t, was less than 1 g. Fifty percent of vertical tail load, L_v, of 5500 lb is indicated at the maximum sideslip angle.

Angle-of-Attack Effect

During the flight test program, concurrent analog studies indicated that increasing or decreasing the angle of attack for roll entries had a considerable effect on the amplitude of the resultant motions. The results of simulator runs made with tail A (C_{n_β} = 0.001/deg) for Mach 0.7 at an altitude of 32,000 ft with varying roll entry initial angles of attack are shown in figure 29 for 1° inclination of the principle axis, ε. The figure shows the envelope of positive and negative increments in the angles of attack and sideslip (Δα and Δβ) as a function of average roll velocity, $\bar{p}$, in left rolls. Data are presented at body axis angles of attack, α = 5°, 1°, and –3° or at angles of attack of the principal axis, ε = ±4° and 0°. The figure illustrates that the roll-coupled motions are a function of the angle of attack of the principal axis rather than the body axis and that increasing the angle of attack of the principal axis for roll entries increases the peak divergences. Maximum divergences occurred near the calculated critical roll velocity of 1.6 rad/sec. Derivation of the principal axis, ε, as a function of the product of inertia, I_{xz}, is shown in appendix E.

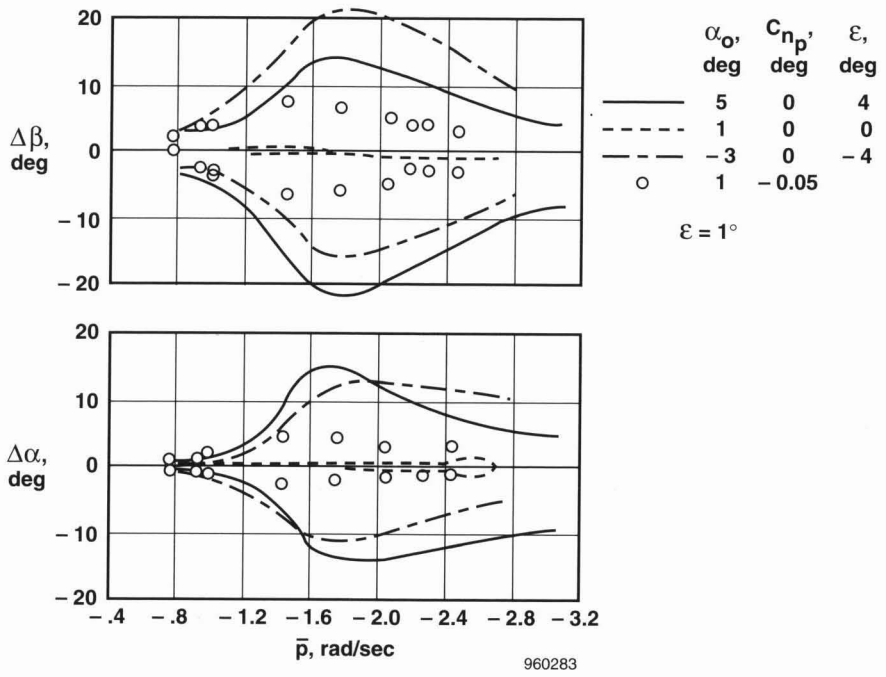

Figure 29. Effect of initial angle of attack of principal axis, ε. Also effect of yaw due to roll velocity, C_{n_p}, during left aileron rolls, Mach 0.7, and pressure altitude 32,000 ft (simulator results).

As shown in figure 29, when the angle of attack of the principal axis for roll entry is zero, essentially no motion is produced. If a yawing moment due to roll velocity, ($C_{n_p} = -0.05$), is introduced, then relatively large incremental peak values are obtained. This effect is not surprising because any yaw will constantly iterate throughout the equations to produce and sustain pitch and yaw coupling through such terms as $p\alpha$, $p\beta$, pr, and pq.

A check on this angle-of-attack effect was made in flight at approximately Mach 0.73 at an altitude of approximately 30,000 ft with tail C for half deflection aileron rolls. Figure 30 indicates that when the angle of attack was reduced from 4° to 2.5°, increments in the angles of attack and sideslip ($\Delta\alpha$ and $\Delta\beta$) decreased.[16] Because a rolling pull-out requires increased g and thus increased angle of attack, this would explain why the early F-100A flight test program rolling pull-outs produced such violent maneuvers. The importance of angle of attack and principal axis as forcing functions in coupled motions is explained in appendix E. The equation for principal axis, ε, is shown in appendix A and developed in appendix E.

Engine Gyroscopics

To assess the effect of jet engine gyroscopics, Phillips' equations[1] were modified to include the moment of inertia and rotor angular velocity of the jet engine.[2,17,18] Figure 31 summarizes piloted simulator studies of the effect of roll direction (Mach 0.7 at an altitude of 30,000 ft; $C_{n_\beta} = 0.001$/deg). In left rolls, the peak motions occur at a lower average roll rate and are 30 percent larger than in the right rolls. Flight tests performed at the same flight conditions confirm the calculated results (fig. 30).

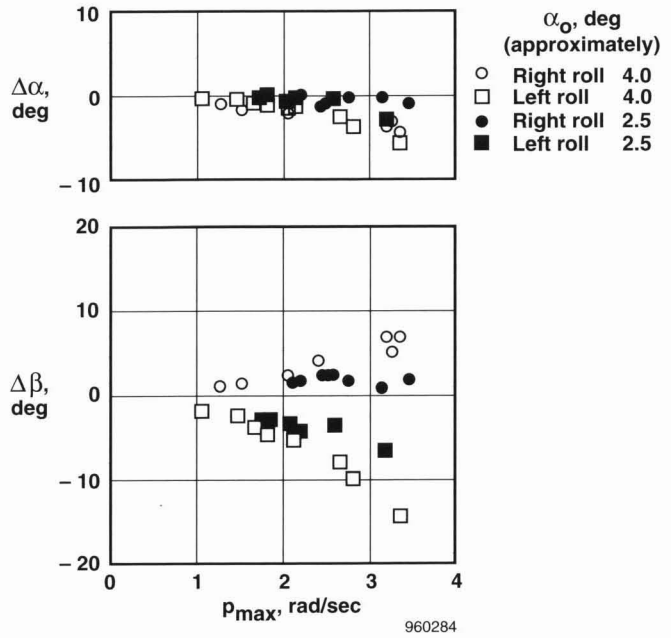

Figure 30. Effect of angle of attack for roll entry on rolling motion of F-100 with tail C at Mach ≈ 0.73 and pressure altitude ≈ 30,000 ft (flight results).[16]

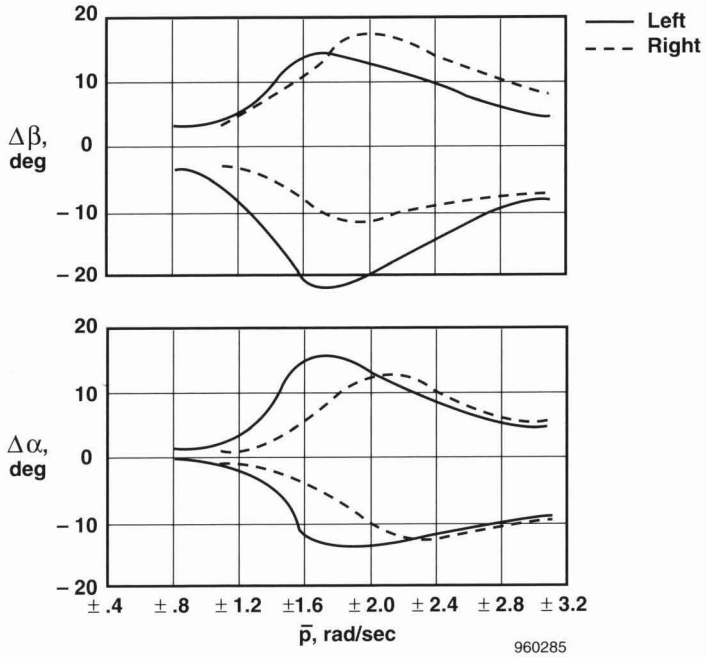

Figure 31. Effect of engine gyroscopics during left and right rolls, F-100A, Mach 0.7, and pressure altitude 30,000 ft (simulator results).

Analog Studies

When the HSFS engineers returned from Langley Research Center, they mechanized** the Edwards Air Force Base GEDA analog simulator for five-degree-of-freedom equations of motion and complemented the flight test

**"Mechanizing" an analog computer is the equivalent of "programming" a digital computer.

program with simulator analyses. (See chapter 4, the F-100A Inertial Roll Coupling section.) The simulator arrangement is as shown in figure 1.

Figure 26(a) illustrates that the two-degree-of-freedom method for calculating longitudinal motions and the three-degree-of-freedom method for calculating lateral–directional motions were not adequate for analyzing the complex inertial and aerodynamic interactions of inertial roll coupling. Several researchers have described the use of the analog simulator for the F-100A flight test guidance and analysis.[14–17,19]

YF-102 INERTIAL ROLL COUPLING

Figures 32(a) and 32(b) show the YF-102 (Convair, San Diego, California). This airplane was the Air Force's first attempt at an all-weather supersonic interceptor and was basically an enlarged XF-92A. The XF-92A did not quite make it chronologically to 100 to become one of the Century series, but it did develop into the YF-102 and contributed to the design of its successors, the F-106 and B-58 aircraft. The YF-102 that arrived at the HSFS in 1954 was used as a test bed for obtaining baseline delta planform data for use in a redesign that incorporated the Whitcomb area rule concept.[3] During this period, the NACA was conducting inertial roll coupling programs on straight wing and swept wing aircraft (X-3 and F-100A) and now had the opportunity to get coupling data on a delta-wing configuration.

It was quite apparent that the airplane had potential coupling problems as can be seen from table 4 which lists the primary coupling ratios for various aircraft. (See also appendix A.) (Coupling tendencies increase as the values approach –1.0.) Based on inertial parameters, the YF-102 has a greater tendency toward coupling than either the X-2 or F-100A.

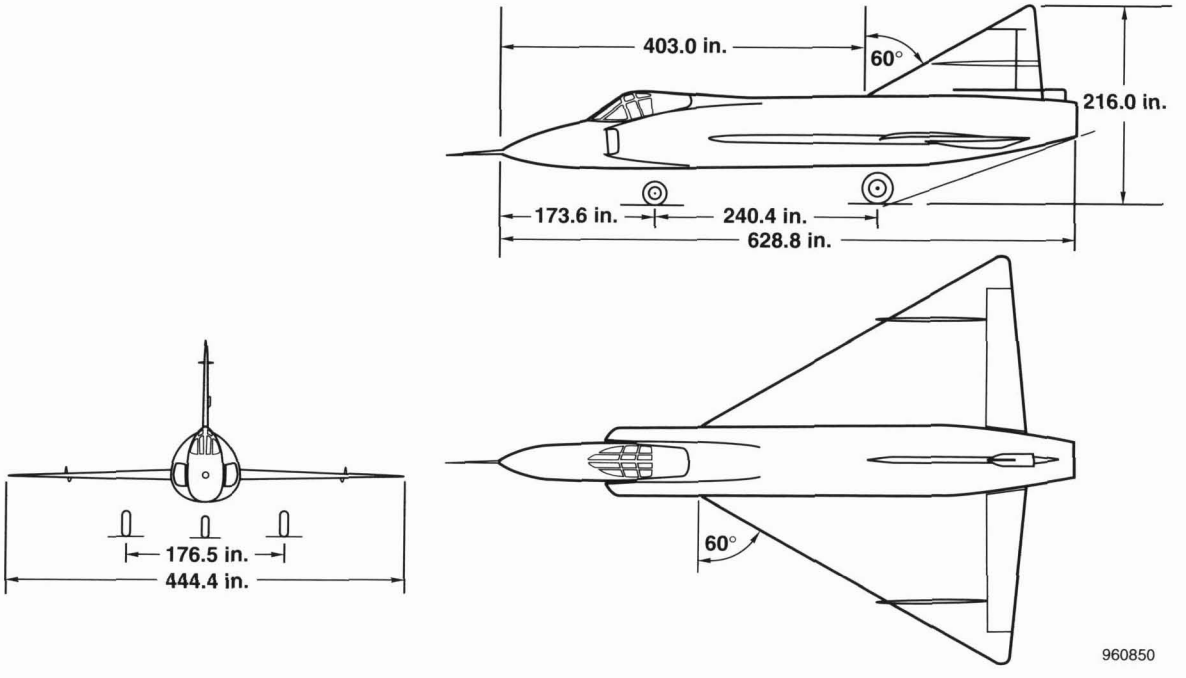

(a) Three-view drawing.

Figure 32. Three view drawing and photograph of the YF-102 airplane.

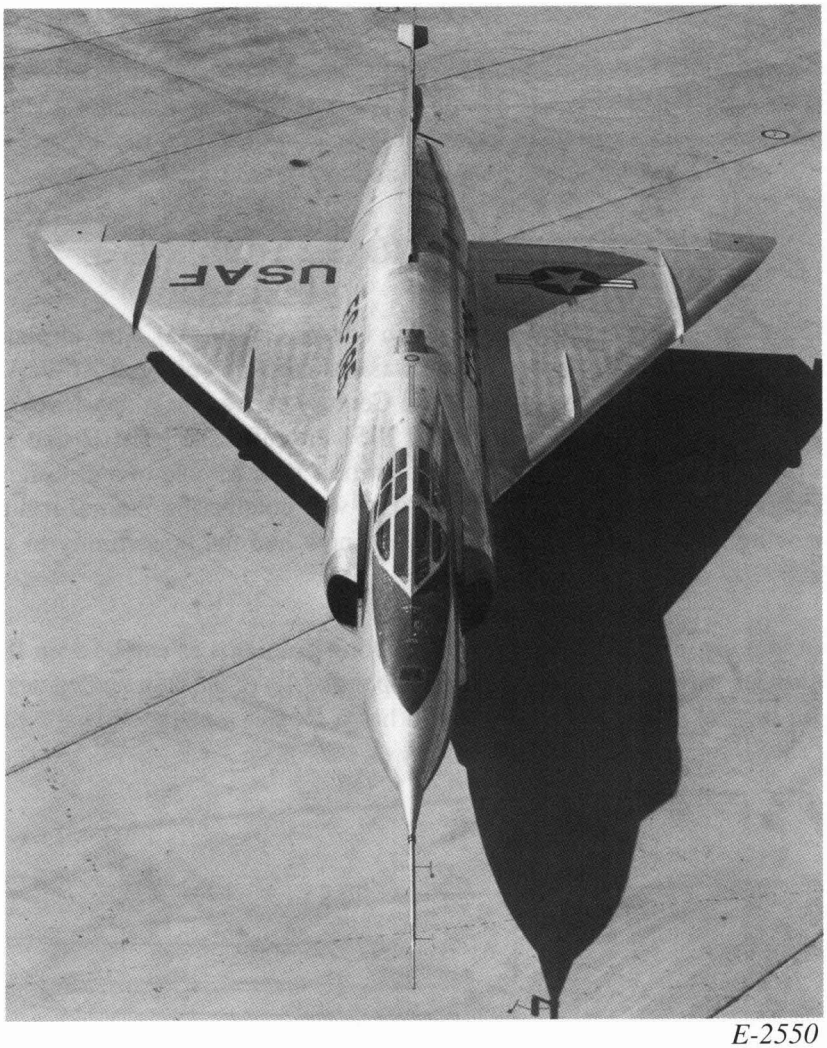

E-2550

(b) Photograph.

Figure 32.Concluded.

Table 4. Primary coupling inertia ratios for various aircraft.

Aircraft	$(I_x - I_y)/I_z$
X-15	–0.94
X-3	–0.88
Shuttle	–0.84
YF-102	–0.81
F-100A	–0.71
X-2	–0.70

YF-102 FLIGHT TEST PROGRAM

Joe Walker, the pilot for the YF-102 airplane during the roll investigations, had been bitten previously in the X-3 aileron roll maneuvers and was aware of the violent coupling behavior of the F-100A aircraft. For these reasons, Walker decided to use a more cautious approach to the YF-102 rolls. He began the program with several rolls in which he terminated the maneuvers at approximately 10° sideslip, and the airplane recovered immediately. In the time history shown in figure 33, an aileron roll was made at a Mach 0.75 and at an altitude of 39,500 ft. The figure showing flight motions and a piloted simulator comparison indicates a large increase in the rate of sideslip buildup at approximately 4 sec at which time the pilot reversed aileron; however, roll rate and sideslip continued to build at ever-increasing rates until sideslip reached a –30° and recorded angle of attack went off scale at –12°. The analog match showed angle of attack more negative than –20°. The motions subsided after the pilot neutralized controls. The simulator arrangement was the same as that shown in figure 1. These divergences were larger than those of the previously discussed YF-100 and X-3 flights; however, because the dynamic pressure was quite low (158 lb/ft^2), excessive loads were not imposed.[19]

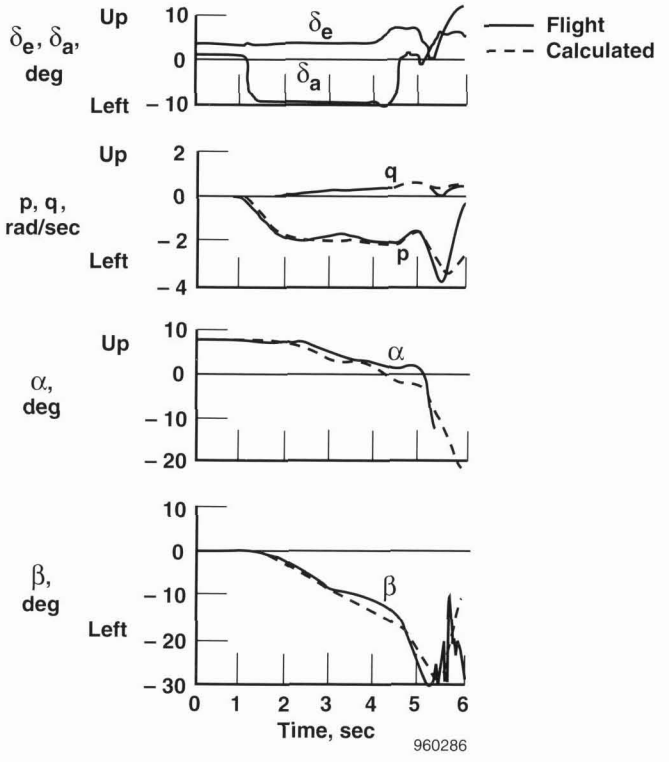

Figure 33. Comparison between flight and calculated roll of the YF-102 airplane, Mach 0.7 and pressure altitude 39,500 ft.

APPENDIX A
MASS PROPERTIES OF COUPLING PRONE AIRCRAFT

Aircraft	X-15	X-3	Shuttle	YF-102	F-100A	X-2
W	14318	21900	198144	30394	23989	12375
m	445	680	6154	944	745	384
I_x	3600	4100	895000	13200	10976	5043
I_y	85000	61200	6918000	106000	57100	25474
I_z	86500	65100	7199000	114600	64975	29106
I_{xz}	–650	4200	167000	3540	942	782
ε	–0.45	3.95	1.52	2.00	1.00	1.86
$(I_y - I_z)/I_x$	–0.42	–0.95	–0.31	–0.65	–0.72	–0.72
$(I_z - I_x)/I_y$	0.98	1.00	0.91	0.96	0.95	0.94
$(I_x - I_y)/I_z$	–0.94	–0.88	–0.84	–0.81	–0.71	–0.70
I_{xz}/I_x	–0.18	1.02	0.19	0.27	0.086	0.16
I_{xz}/I_y	–0.0076	0.069	0.024	0.033	0.017	0.031
I_{xz}/I_z	–0.0075	0.065	0.023	0.031	0.014	0.027
I_z/I_x	24.0	15.9	8.0	8.7	5.9	5.8

where $\varepsilon = 57.3\dfrac{I_{xz}}{I_z - I_x}$, deg

APPENDIX B
FIVE-DEGREE-OF-FREEDOM EQUATIONS OF MOTION (REFERENCED TO BODY AXES)

$$\dot{p} = \left(\frac{I_y - I_z}{I_x}\right)qr + \frac{I_{xz}}{I_x}\dot{r} + \frac{I_{xz}}{I_x}pq + \frac{Ab}{I_x}C_{l_\beta}\beta + \frac{Ab}{I_x}C_{l_{\delta_a}}\delta_a + \frac{Ab}{I_x}C_{l_{\delta_r}}\delta_r + \frac{Ab^2}{2VI_x}C_{l_p}p + \frac{Ab^2}{2VI_x}C_{l_r}r$$

$$\dot{q} = \left(\frac{I_z - I_x}{I_y}\right)pr + \frac{I_{xz}}{I_y}r2 - \frac{I_{xz}}{I_y}p2 - \frac{I_{x_e}\omega_e}{I_y}r + \frac{A\bar{c}}{I_y}C_{m_\alpha}\Delta\alpha + \frac{A\bar{c}}{I_y}C_{m_{\delta_e}}\delta_e + \frac{A\bar{c}^2}{2VI_y}C_{m_q}q$$

$$\dot{r} = \left(\frac{I_x - I_y}{I_z}\right)pq + \frac{I_{xz}}{I_z}\dot{p} - \frac{I_{xz}}{I_z}qr + \frac{I_{x_e}\omega_e}{I_z}q + \frac{Ab}{I_z}C_{n_\beta}\beta + \frac{Ab}{I_z}C_{n_{\delta_r}}\delta_r + \frac{Ab}{I_z}C_{n_{\delta_a}}\delta_a + \frac{Ab^2}{2VI_z}C_{n_r}r + \frac{Ab^2}{2VI_z}C_{n_p}p$$

$$\dot{\beta} = \frac{g}{V}\sin\varphi\cos\theta - r\cos\alpha + p\sin\alpha + \frac{A}{mV}C_{Y_\beta}\beta$$

$$\dot{\alpha} = \frac{g}{V}\cos\varphi\cos\theta + q - p\sin\beta - \frac{A}{mV}C_{L_\alpha}\alpha$$

where $A = \dfrac{\rho V^2 S}{2} = \bar{q}S$.

These equations contain all the first-order terms required for coupling analyses and derivations in the text and appendixes. The following shows a breakdown of contributing aerodynamic and inertial factors in the yawing moment equation:

Aerodynamic				Inertial	
Stability	Control	Damping		Gyroscopic	Centrifugal
$N_\beta\beta$	$+ N_{\delta_r}\delta_r + N_{\delta_a}\delta_a$	$+ N_r r + N_p p$	$=$	$I_z\dot{r} - (I_x - I_y)pq - I_{x_e}\omega_e q$	$+ I_{xz}(qr - \dot{p})$

APPENDIX C
STATIC CONTROL COUPLING

Coupling of lateral–directional stability and control derivatives

In the examples of control coupling discussed in chapters 1, 2, and 3, a directional controller was not used. The rudder was locked on the X-2, adverse for the X-15, or ineffective for the Space Shuttle. Only the ailerons (X-2), rolling tail (X-15),[††] or elevons (Shuttle) were available for lateral–directional control.

Neutral static control is obtained by setting the $\dot{p}$ and $\dot{r}$ equations of appendix B to zero and removing insignificant or irrelevant terms.

$$I_x\dot{p} = (I_y - I_z)qr + \bar{q}SbC_{l_{\delta_a}}\delta_a + \bar{q}SbC_{l_\beta}\beta = 0$$

$$I_y\dot{r} = (I_x - I_y)qp + \bar{q}SbC_{n_{\delta_a}}\delta_a + \bar{q}SbC_{n_\beta}\beta = 0$$

For lateral–directional control, pitching velocity, q, is assumed to be negligible. Clearing the above,

$$C_{l_{\delta_a}}\delta_a = -C_{l_\beta}\beta$$

$$C_{n_{\delta_a}}\delta_a = -C_{n_\beta}\beta$$

Dividing equals by equals gives the balance equation or "control parameter" for neutral control as discussed in chapter 1.

$$\frac{C_{n_\beta}}{C_{n_{\delta_a}}} = \frac{C_{l_\beta}}{C_{l_{\delta_a}}}$$

Rearranging, as shown below, indicates that the left-hand side of the equation must be greater than 1 for proverse or stable control. This parameter is plotted as a function of Mach number in chapter 1, figure 5(b) for two X-2 flights.

$$\frac{C_{n_\beta}C_{l_{\delta_a}}}{C_{l_\beta}C_{n_{\delta_a}}} > 1.0$$

The control parameter is rearranged and expressed in yet another form in chapter 3, table 2, to indicate the large, unaugmented adverse control of the Space Shuttle during entry. In this form, the parameter indicates that the directional stability coefficient must be greater than the right-hand side of the inequality.

$$C_{n_\beta} > \frac{C_{n_{\delta_a}}C_{l_\beta}}{C_{l_{\delta_a}}}$$

[††]Dynamic control coupling of the X-15 is described in chapter 2.

APPENDIX D
DUTCH ROLL COUPLING

Recognition of the impact of dutch roll stability in high-speed aircraft
Historical development of the dutch roll stability equation

Dutch roll coupling is dynamic lateral–directional stability of the stability axis. This coupling of body axis yaw and roll moments with sideslip can produce lateral–directional instability or PIO. This coupling can also stabilize an aircraft with unstable body axes.

Before the early 1950's, dutch roll was a familiar occurrence. However, with the fairly even distribution of inertias and high values of stability and damping, dutch roll was perhaps at times an annoyance, but it was not considered a severe problem. The more pronounced dutch roll coupling appeared as a by-product of the post-WWII era of technological progress which produced mass concentration in fuselages and decreased damping with increased speed and altitude. The primary aircraft affected were experimental research aircraft, the Century series military aircraft and the Shuttle.

Derivation of the dutch roll equation is not a recent development; it has been around for quite some time. However, until the mid-1950's, the body-axis directional stability, C_{n_β}, was calculated from the dutch roll (stability axis) frequency. These calculations neglected the influence of inertia ratios, angle of attack, and effective dihedral.

During this period, values of C_{n_β} obtained from flight data were almost invariably less than the wind-tunnel values and, as so frequently happens when discoveries are made, several engineers almost simultaneously, and independently, associated the inertial properties, angle of attack, and body axis stability with dutch roll frequency and derived the dutch roll equation as shown below:

Dimensional derivative form, $\omega_d{}^2 = \dfrac{N^*_\beta}{I_z} = \dfrac{N_\beta}{I_z}\cos\alpha_0 - \dfrac{L_\beta}{I_x}\sin\alpha_0$

Nondimensional derivative form, $C_{n_\beta}{}^* = C_{n_\beta}\cos\alpha_0 - \dfrac{I_z}{I_x}C_{l_\beta}\sin\alpha_0$

Because C_{n_β} was the prime factor in assessing lateral–directional stability, engineers retained the familiar terminology and labeled the stick-fixed dutch roll stability "C_{n_β} dynamic," or as a shorthand symbol, "$C_{n_\beta}{}^*$" Although incorrect in that it is a combination of yaw and roll coefficients, this nomenclature became a part of the engineering terminology in the mid-1950's and remains in use today.

DERIVATION OF DUTCH ROLL STABILITY EQUATION

Coupled stability and control equations are usually derived from the roots of determinants using classical stability criteria. However, it is interesting to note the different methods used by different authors for arriving at the dutch roll equation from the three lateral–directional equations of motion. For example,

- 1955, Banner and Kuhl—differentiation of the $\dot{\beta}$ equation and solve simultaneously[15‡‡]
- 1955, Wolowicz—trigonometric transfer of stability axes to body axes[§§]
- 1959, Pine—determinant roots[¶¶]

Regardless of the different approaches, the math and physics are the same. The equations of motion are shown in appendix B. The only derivation in appendix D will be that of Banner and Kuhl.

BANNER AND KUHL DIFFERENTIATION METHOD, 1955

The above form of the dutch roll equation as used in flight test was first derived and reported by Banner and Kuhl on March 11, 1955,[‡‡] and later that year the derivation was repeated in reference 14 and used to determine the flight test values of C_{n_β} for the F-100A inertial roll coupling program as discussed in chapter 4. Banner and Kuhl's derivation was somewhat unique in that they differentiated the $\dot{\beta}$ equation with respect to time then they simultaneously solved the lateral–directional equations of motion. These authors first reduced the lateral–directional equations to their simplest form by

- assuming angle of attack at which the oscillation is initiated is constant;
- assuming $\sin\alpha = \alpha$ and $\cos\alpha = 1$ for moderate angles of attack;
- eliminating the terms divided by V (rotary, gravity, and force terms); and
- considering the XZ product of inertia negligible.

This reduces the lateral–directional equations to

$$\dot{p} = L_\beta \beta / I_x$$

$$\dot{r} = N_\beta \beta / I_z$$

$$\dot{\beta} = -r + \alpha_0 p$$

Then, taking the time derivative of the $\dot{\beta}$ equation,

$$\ddot{\beta} = -\dot{r} + \alpha_0 \dot{p} = -\frac{N_\beta \beta}{I_z} + \alpha_0 \frac{L_\beta \beta}{I_x} = \left(-\frac{N_\beta}{I_z} + \alpha_0 \frac{L_\beta}{I_x}\right)\beta$$

$$\ddot{\beta} + \left(\frac{N_\beta}{I_z} - \alpha_0 \frac{L_\beta}{I_x}\right)\beta = 0$$

‡‡Banner, Richard D. and Kuhl, Albert E. "The Determination of the Directional Stability Parameter, C_{n_β}, from Flight Data," unpublished memorandum for Engineering Division Chief, NACA HSFS, Edwards, California, March 11, 1955.

§§Wolowicz, Chester H., "Some Notes on the Transformation of Derivatives and Moments of Inertia from One System of Axes to Axes of Another," unpublished working paper, NACA HSFS, Edwards, California, 1955.

¶¶Pine, A., "Lateral–Directional Static Stability Criteria for High Velocity and Altitude," interoffice letter to manager W.E. Swanson, North American Aviation, Inc., Los Angeles, California, July 17, 1959.

using the differential operator D, $D^2 = -\left(\frac{N_\beta}{I_z} - \alpha_0 \frac{L_\beta}{I_x}\right)$

The natural frequency of the oscillation ω_d is determined from the imaginary part of the roots.

$$D = \omega_d = i\sqrt{-\left(\frac{N_\beta}{I_z} - \alpha_0 \frac{L_\beta}{I_x}\right)}, \text{ squaring, } {\omega_d}^2 = \frac{N_\beta^*}{I_z} = \frac{N_\beta}{I_z} - \alpha_0 \frac{L_\beta}{I_x}$$

Nondimensionalizing and solving for C_{n_β} gives the equation

$$C_{n_\beta} = C_{n_\beta}^* + \alpha_0 \frac{I_z}{I_x} C_{l_\beta}, \text{ solving for } C_{n_\beta}^*$$

$$C_{n_\beta}^* = C_{n_\beta} - \alpha_0 \frac{I_z}{I_x} C_{l_\beta}$$

The entry angles of attack could be on the order of 25° for the X-15 and 40° for the Space Shuttle. For these magnitudes, the trigonometric forms of angle of attack should be applied making the dutch roll derivative,

$$C_{n_\beta}^* = C_{n_\beta} \cos\alpha_0 - \frac{I_z}{I_x} C_{l_\beta} \sin\alpha_0$$

In the above equation, it is seen that the necessary and sufficient condition for lateral–directional static stability is

$$C_{n_\beta} \cos\alpha_0 > -\frac{I_z}{I_x} C_{l_\beta} \sin\alpha_0 \text{ or } C_{n_\beta} > \frac{I_z}{I_x} C_{l_\beta} \tan\alpha_0$$

This condition clearly indicates why heavily loaded fuselages and appreciable angles of attack have such a powerful effect on lateral–directional stability. See appendix A for I_z/I_x values of the six aircraft discussed in the text.

ADDITIONAL NOTES CONCERNING DUTCH ROLL

The term "dutch roll" is said to come from watching the rolling and swinging motions of a Dutchman ice skating. Another description of the motion is that of a ball bearing rolling inside a barrel. After experiencing a particularly annoying dutch roll, the NACA/NASA test pilot Joe Walker described the motion as a ball bearing rolling on the *outside* of a barrel.

Determining body axis (static) directional stability from the dutch roll frequency was required for the following:

- to check the validity of wind-tunnel data (wind tunnels measure static forces),
- to modify aircraft for desired stability,
- to provide accurate data for programming simulators, and
- to provide accurate data for programming flight control systems.

Dutch roll with adverse effective dihedral can produce uncontrollability as described for the X-15 in chapter 2.

Dutch roll can generate PIO when positive effective dihedral produces high roll-to-yaw oscillations.

The terms on the right-hand side of the dutch roll equation for the X-15 were the reverse of those for the Space Shuttle:

	C_{n_β}	C_{l_β}
X-15	+	−
Shuttle	−	+

These effects are described in chapters 2 and 3.

APPENDIX E
INERTIAL ROLL COUPLING

An airplane rolling about an axis that is not aligned with the principal axis develops a resonant divergence in pitch or yaw when the roll rate is equal to the lower of the pitch or yaw natural frequencies.

The primary source of information for the following analysis is from Phillips' NACA Technical Note published in 1948.[1] Some minor modifications to the analysis were taken from reference 17.

In order to show the primary effects of the rolling motion, the following simplifying assumptions are made to the five-degree-of-freedom equations shown in appendix B:

- $\dot{p} = 0$, p = constant, reducing the derivation to four degrees of freedom.
- p_0 = steady rolling velocity.
- Terms divided by V (gravity, damping, and force) are deleted.
- The product of inertia $I_{xz} = 0$.
- $\sin\theta = \theta$, $\cos\theta = 1$, $\sin\psi = \psi$.
- ω_θ and ω_ψ are the nondimensional ratios of undamped, natural frequencies in pitch and yaw to steady rolling frequency, p_0.

As shorthand notation, $(I_x - I_y)/I_z = F$; and $(I_z - I_x)/I_y = F'$. Considering these assumptions, the five-degrees of freedom are reduced to the following four:

$$\dot{q} - rp_0F' + \omega_\theta{}^2\theta = 0$$

$$\dot{r} + qp_0F + \omega_\psi{}^2\psi = 0$$

$$\dot{\theta} = q + \psi p_0, \text{ or } q = \dot{\theta} - \psi p_0$$

$$\dot{\psi} = r - \theta p_0, \text{ or } r = \dot{\psi} + \theta p_0$$

If these substitutions are made, these equations become

$$\ddot{\theta} - p_0\dot{\psi} - (p_0\dot{\psi} + p_0^2\theta)F' + \omega_\theta{}^2p_0^2\theta = 0$$

$$\ddot{\psi} + p_0\dot{\theta} + (p_0^2\psi - p_0\dot{\theta})F + \omega_\psi{}^2p_0^2\psi = 0$$

Using the differential operator D, the determinant of the equations is

$$\begin{vmatrix} D^2 - F' + \omega_\theta{}^2 & -D - DF' \\ D - DF & (D^2 + F + \omega_\psi)^2 \end{vmatrix}$$

The determinant, when expanded, gives the quartic

$$aD^4 + cD^2 + e = 0$$

where

$$a = 1$$

$$c = 1 - FF' + \omega_\psi{}^2 + \omega_\theta{}^2$$

and

$$e = -FF' + \omega_\theta{}^2\omega_\psi{}^2 - F'\omega_\psi{}^2 + \omega_\theta{}^2 F$$

The divergence boundary is obtained by setting the coefficient $e = 0$.

$$e = -FF' + \omega_\theta{}^2\omega_\psi{}^2 - F'\omega_\psi{}^2 + \omega_\theta{}^2 F = 0$$

factoring

$$(F' - \omega_\theta{}^2)(-F - \omega_\psi{}^2) = 0$$

and

$$\omega_\theta{}^2 = F' \; ; \; \omega_\psi{}^2 = -F$$

If $\omega_\theta{}^2$ and $\omega_\psi{}^2$ are plotted as ordinate and abscissa, it is seen that a stability plot can be obtained similar to those in Phillips' report.[1] Neutral stability boundaries are shown as F' and $-F$. Regions free from divergence are indicated by the cross-hatching.

Solving for the value of the positive real root D of the above quadratic in D^2 will determine the nondimensional time to double amplitude in accordance with the equation

$$t' = \frac{0.693}{\text{positive real root}}$$

where t' is the nondimensional time to double amplitude.

Consider the specified points in the unstable portion of the following stability chart (fig. E-1):

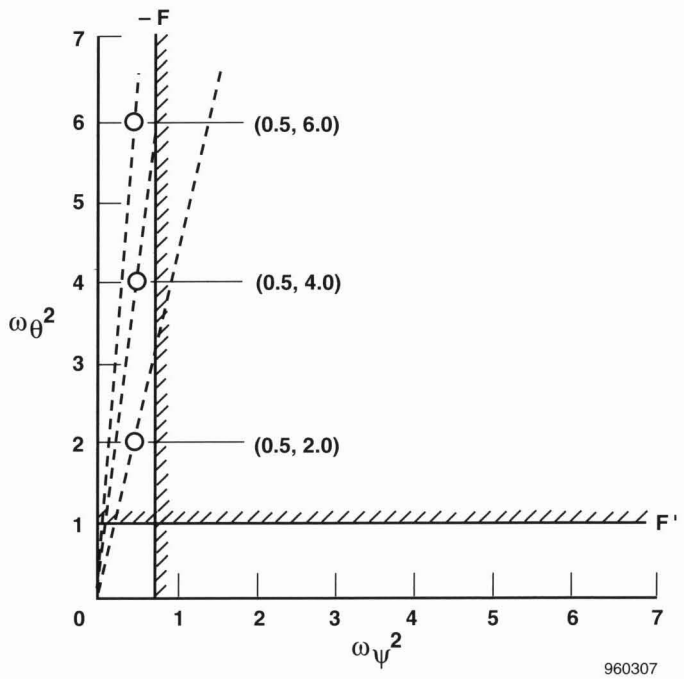

Figure E-1. Stability diagram for constant rolling aircraft. Stable side of boundaries indicated by cross-hatching.

If $-F = 0.71$ and $F' = 0.95$ (the values for the inertia ratios of the F-100A airplane as shown in appendix A), then the positive real root for the points considered will be as follows:

ω_ψ^2	ω_θ^2	Positive real root	t'
0.5	2.0	0.228	3.03
0.5	4.0	0.319	2.17
0.5	6.0	0.357	1.94

Thus, it would be expected that if the vertical displacement of the three points considered is caused by increased C_{m_α} (the rate of roll being identical), the rate of divergence would increase as the location of the point in the unstable region increased.

The diagram also indicates that an optimum condition exists when the resonant frequencies in pitch and yaw are approximately equal. This also means that the larger the absolute values of the inertia ratios $(I_x - I_y)/I_z$ and $(I_z - I_x)/I_y$, the more susceptible the aircraft is to divergence at resonant roll frequencies. Because roll about the principal axis rather than the body axis is the forcing function for producing resonant divergences, an appreciation of the relationship between body and principal axes is desirable.

DETERMINATION OF THE ANGLE OF INCLINATION OF THE PRINCIPAL AXIS, ε, IN TERMS OF BODY AXIS MOMENTS OF INERTIA.

The principal axes of a body through a given point are axes of maximum or minimum moments of inertia, or a principal axis of an object is an axis about which the object could be rotated freely through the center of mass with no rotation about either of the other two principal axes (fig. E-2).

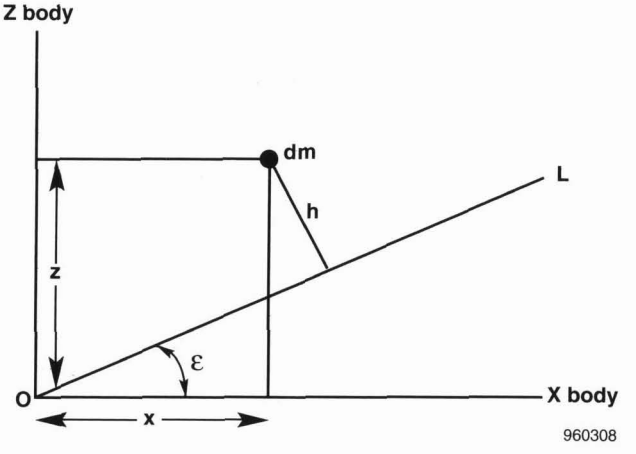

Figure E-2. Diagram for determining principal moment of inertia about the line OL.

In the XZ plane of symmetry of figure E-2, the moment arm, h, from OL to dm is

$$h = z\cos\varepsilon - x\sin\varepsilon$$

The moment of inertia, I_L, about axis *OL* through the center of mass becomes

$$I_L = \int h^2 dm = \int (z^2 \cos^2 \varepsilon + x^2 \sin^2 \varepsilon - 2xz \cos \varepsilon \sin \varepsilon) dm$$

Substituting the trigonometric identity, $2\cos\varepsilon\sin\varepsilon = \sin 2\varepsilon$,

$$I_L = I_x \cos 2\varepsilon + I_z \sin 2\varepsilon - I_{xz} \sin 2\varepsilon$$

For *OL* to represent the principal axis, I_L must be at minimum value; therefore, its derivative with respect to ε must be zero. That is,

$$-2I_x \cos\varepsilon \sin\varepsilon + 2I_z \sin\varepsilon \cos\varepsilon + 2I_{xz} \cos 2\varepsilon = 0$$

Again, using the above identity,

$$-I_x \sin 2\varepsilon + I_z \sin 2\varepsilon + I_{xz} \cos 2\varepsilon = 0$$

Dividing by $\cos 2\varepsilon$, simplifying and solving for ε gives

$$\tan 2\varepsilon = -2I_{xz}/(I_z - I_x)$$

The diagram shows the body axis below the axis *OL*. When the body axis is above the principal axis at the nose, the right-hand side of the above equation becomes positive. Also, the principal axes of high-performance aircraft are sufficiently small that $\tan 2\varepsilon = 2\varepsilon$, and the angle of inclination of the principal axis becomes

$$\varepsilon = I_{xz}/(I_z - I_x) \text{ rad}$$

(positive when the body axis is above the principal axis at the nose). Appendix A lists ε for the six aircraft discussed in this report. Note that ε cannot be used as an arbitrary number in simulator or control system math models because the angle is a function of the body axis inertias I_{xz}, I_z, and I_x.

MECHANICAL ROLL COUPLING DEMONSTRATOR

In 1955, the NACA machine shop fabricated a mechanical model for demonstrating various aspects of inertial roll coupling (fig. E-3). The model had the following capabilities:

- The crank, shown on the left, rotated the inertial model about the roll axis of a three-gimbaled framework that permitted the model to respond to inertial moments about pitch and yaw axes.
- The springs on bars above and below the model could be adjusted to vary pitch and yaw stability (frequency).
- The adjustable weights on the bar running along the centerline of the model could be positioned fore and aft to vary the moments of inertia about the pitch and yaw axes and still maintain the center of mass at the pivot. This bar could also be rotated in pitch to vary the product of inertia and thus the angle of incidence of the principal axis.
- The boom on the nose of the model indicated the degree of divergence on the circularly engraved target.

When the crank was turned at a roll frequency equal to the lower frequency of pitch or yaw, resonance would occur to produce a divergence in that axis. The model shown in the photograph was presented by NASA to the Test Pilot's School at the Air Force Flight Test Center, Edwards, California, and is now used to demonstrate inertial roll coupling to test pilot students.

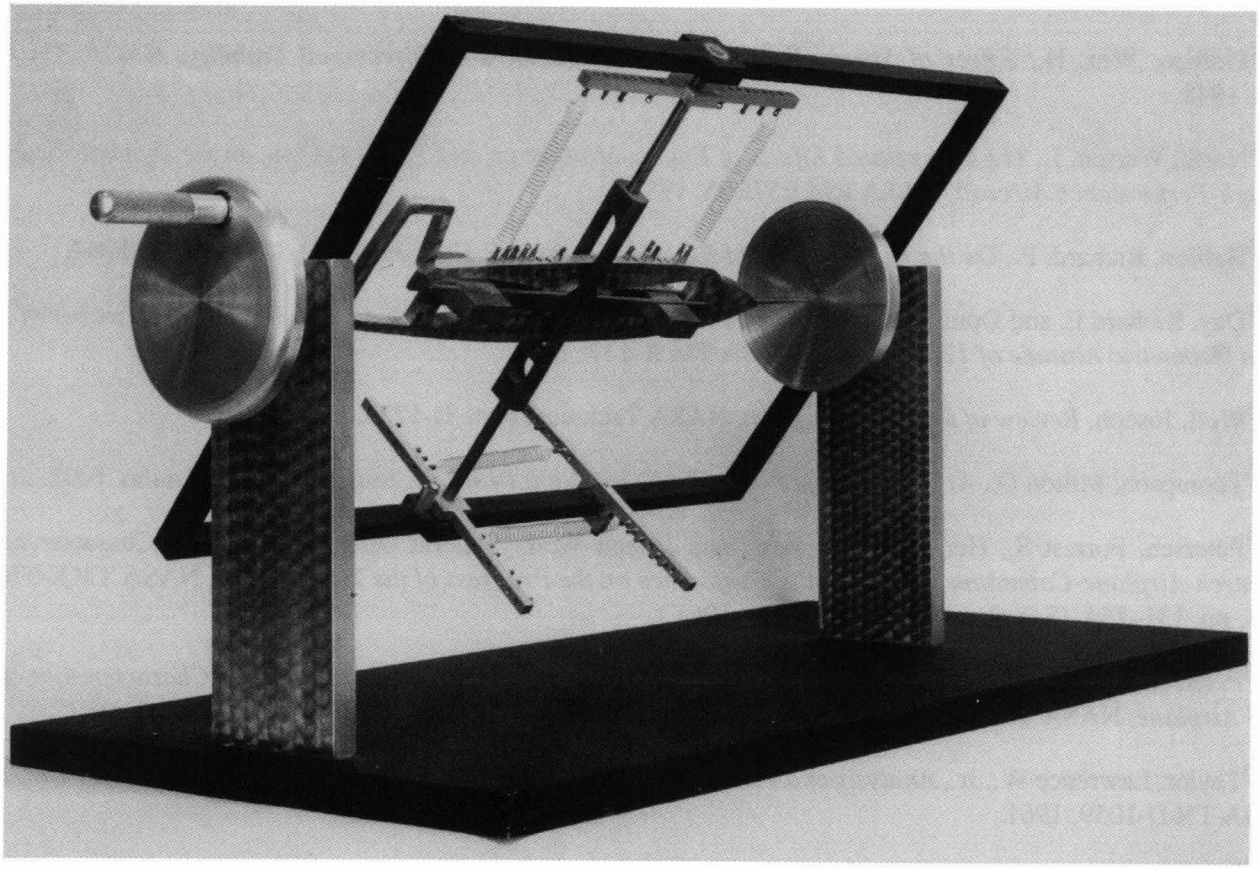

NACA E-4231

Figure E-3. Mechanical model for demonstrating inertial roll coupling.

REFERENCES

[1]Phillips, Wm. H., *Effect of Steady Rolling on Longitudinal and Directional Stability*, NACA TN 627, June, 1948.

[2]North, Warren, J., *The Interrelated Effects of Engine Momentum and Flight Regime on the Dynamic Stability of High-Performance Aircraft*, NASA RM E57B05, 1957.

[3]Hallion, Richard, P., *On the Frontier, Flight Research at Dryden 1946-1981*, NASA SP-4303, 1984.

[4]Day, Richard E. and Donald Reisert, *Flight Behavior of the X-2 Research Airplane to a Mach Number of 3.20 and a Geometric Altitude of 126,200 Feet*, NASA TM X-137, 1959.

[5]Weil, Joseph, *Review of the X-15 Program*, NASA Technical Note D-1278, 1962.

[6]Thompson, Milton O., *At the Edge of Space: The X-15 Flight Program*, Smithsonian Institution, 1992.

[7]Petersen, Forrest S., Herman A. Rediess, and Joseph Weil, "Lateral Directional Control Characteristics," *Research-Airplane-Committee Report on the Conference on the Progress of the X-15 Project*, NASA TMX-57072, 1961, pp. 131–154. (See also NASA TMX-726, 1961.)

[8]Petersen, Forrest S., Herman A. Rediess, and Joseph Weil, *Lateral–Directional Control Characteristics of the X-15 Airplane*, NASA TM X 726, 1962.

[9]Taylor, Lawrence W., Jr., *Analysis of a Pilot-Airplane Lateral Instability Experienced with the X-15 Airplane*, NASA TN D-1059, 1961.

[10]Rockwell International, "Aerodynamic Design Data Book," *Orbiter Vehicle 102 (ADDB-I)*, vol. 1, SD 72-SH-0060-IJ, June 25, 1976.

[11]Iliff, Kenneth W. and Mary F. Shafer, *Space Shuttle Hypersonic Aerodynamic and Aerothermodynamic Flight Research and the Comparison to Ground Test Results*, NASA TM 4499, 1993.

[12]NACA High Speed Flight Station, *Flight Experience with Two High-Speed Airplanes Having Violent Lateral–Longitudinal Coupling in Aileron Rolls*, NACA RM H55A13, 1955.

[13]Day, Richard E. and Jack Fischel, *Stability and Control Characteristics Obtained During Demonstration of the Douglas X-3 Research Airplane*, NACA RM H55E16, 1955.

[14]Weil, Joseph, Ordway B. Gates, Jr., Richard D. Banner, and Albert E. Kuhl, *Flight Experience of Inertia Coupling in Rolling Maneuvers*, NACA RM H55E17b, 1955.

[15]Drake, Hubert M., Thomas W. Finch, and James R. Peele, *Flight Measurements of Directional Stability to a Mach Number of 1.48 for an Airplane Tested with Three Different Vertical Tail Configurations*, NACA RM H55G26, 1955.

[16]Finch, Thomas W., James R. Peele, and Richard E. Day, *Flight Investigation of the Effect of Vertical-Tail Size on the Rolling Behavior of a Swept-Wing Airplane Having Lateral–Longitudinal Coupling*, NACA RM H55L28a, 1956.

[17]Weil, Joseph and Richard E. Day, *An Analog Study of the Relative Importance of Various Factors Affecting Roll Coupling*, NACA RM H56A06, 1956.

[18]Gates, Ordway B., Jr., and C.H. Woodling, *A Theoretical Analysis of the Effect of Engine Angular Momentum on Longitudinal and Directional Stability in Steady Rolling Maneuvers*, NACA RM L55G05, 1955.

[19]Weil, Joseph and Richard E. Day, *Correlation of Flight and Analog Investigations of Roll Coupling*, NACA RM H56F08, 1956.

REPORT DOCUMENTATION PAGE

Form Approved
OMB No. 0704-0188

1. AGENCY USE ONLY (Leave blank)	2. REPORT DATE	3. REPORT TYPE AND DATES COVERED
	March 1997	Special Publication

4. TITLE AND SUBTITLE

Coupling Dynamics in Aircraft: A Historical Perspective

5. FUNDING NUMBERS

WU-953-36-00

6. AUTHOR(S)

Richard E. Day

7. PERFORMING ORGANIZATION NAME(S) AND ADDRESS(ES)

NASA Dryden Flight Research Center
P.O. Box 273
Edwards, California 93523-0273

8. PERFORMING ORGANIZATION REPORT NUMBER

H-2106

9. SPONSORING/MONITORING AGENCY NAME(S) AND ADDRESS(ES)

National Aeronautics and Space Administration
Washington, DC 20546-0001

10. SPONSORING/MONITORING AGENCY REPORT NUMBER

NASA SP-532

11. SUPPLEMENTARY NOTES

Richard E. Day (NASA retired). Prepared under NASA contract NASA 2-13445, subcontract no. TSD-93-RED-2805.

12a. DISTRIBUTION/AVAILABILITY STATEMENT

Unclassified—Unlimited
Subject Category 08

12b. DISTRIBUTION CODE

13. ABSTRACT (Maximum 200 words)

Coupling dynamics can produce either adverse or beneficial stability and controllability, depending on the characteristics of the aircraft. This report presents archival anecdotes and analyses of coupling problems experienced by the X-series, Century series, and Space Shuttle aircraft. The three catastrophic sequential coupling modes of the X-2 airplane and the two simultaneous unstable modes of the X-15 and Space Shuttle aircraft are discussed. In addition, the most complex of the coupling interactions, inertia roll coupling, is discussed for the X-2, X-3, F-100A, and YF-102 aircraft. The mechanics of gyroscopics, centrifugal effect, and resonance in coupling dynamics are described. The coupling modes discussed are interacting multiple degrees of freedom of inertial and aerodynamic forces and moments. The aircraft are assumed to be rigid bodies. Structural couplings are not addressed. Various solutions for coupling instabilities are discussed.

14. SUBJECT TERMS

Coupling dynamics; Coupling modes; F-100 aircraft; Space Shuttle; X-2 aircraft; X-3 aircraft; X-15 aircraft; YF-102 aircraft.

15. NUMBER OF PAGES

71

16. PRICE CODE

AO4

17. SECURITY CLASSIFICATION OF REPORT	18. SECURITY CLASSIFICATION OF THIS PAGE	19. SECURITY CLASSIFICATION OF ABSTRACT	20. LIMITATION OF ABSTRACT
Unclassified	Unclassified	Unclassified	Unlimited

NASA Special Publication 532

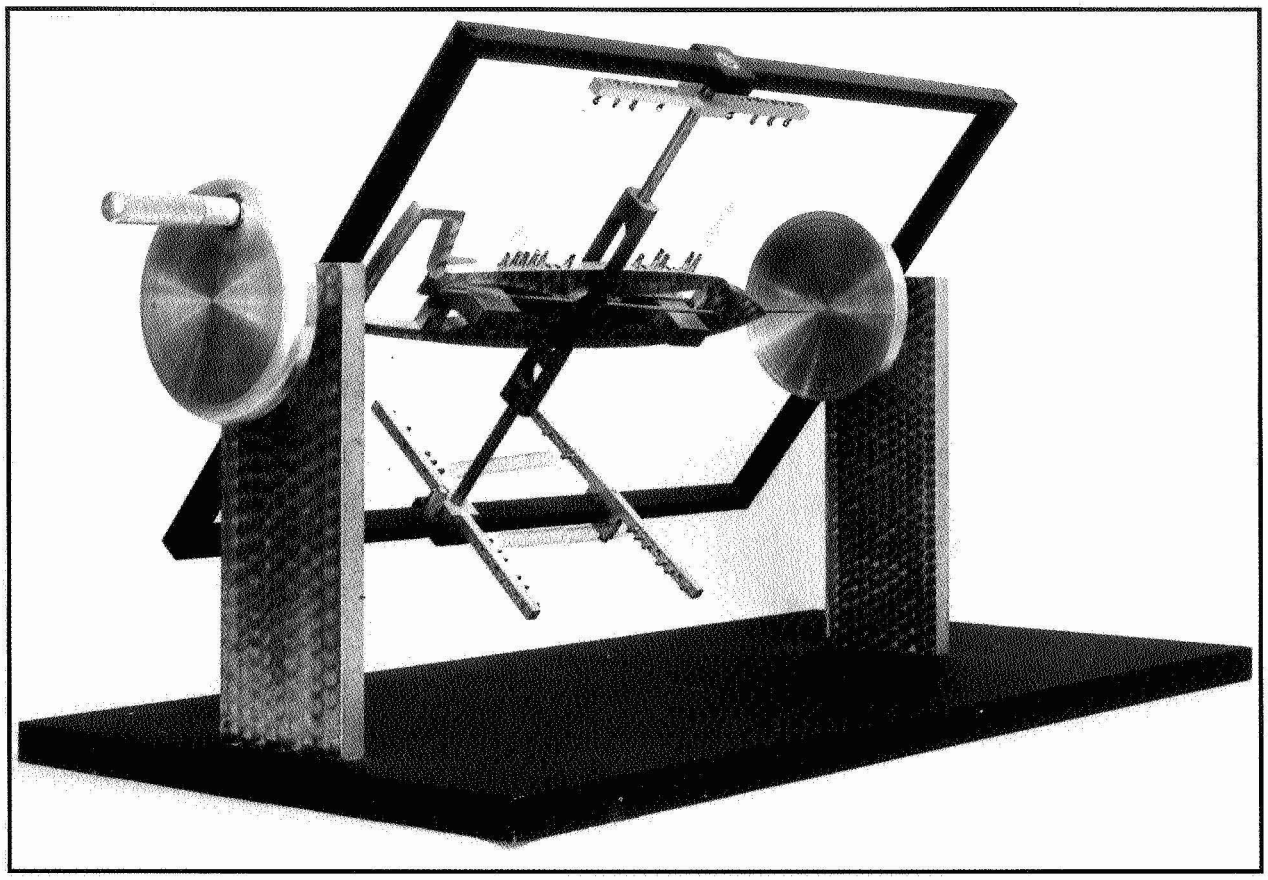

National Aeronautics and
Space Administration

Dryden Flight Research Center
P.O. Box 273
Edwards, Ca. 93523-0273